Electron Beam Ion Sources

G. Zschornack[a,b], M. Schmidt[b] and A. Thorn[b]
[a]University of Technology Dresden, Helmholtz-Zentrum Dresden-Rossendorf, Dresden, Germany
[b]Dreebit GmbH, Dresden, Germany

Abstract

Electron beam ion sources (EBISs) are ion sources that work based on the principle of electron impact ionization, allowing the production of very highly charged ions. The ions produced can be extracted as a DC ion beam as well as ion pulses of different time structures. In comparison to most of the other known ion sources, EBISs feature ion beams with very good beam emittances and a low energy spread. Furthermore, EBISs are excellent sources of photons (X-rays, ultraviolet, extreme ultraviolet, visible light) from highly charged ions. This chapter gives an overview of EBIS physics, the principle of operation, and the known technical solutions. Using examples, the performance of EBISs as well as their applications in various fields of basic research, technology and medicine are discussed.

1 Introduction

The idea to develop electron beam ion sources (EBISs) was constituted by the need for multiply charged ions for accelerator applications to derive high final particle kinetic energies and by a general scientific interest to study exotic states of matter as represented by highly charged ions (HCIs).

Highly charged ions possess properties that differ in many ways from atoms and low charged ions. The following are some of the distinguishing characteristics.

- Due to the ionization process, a large amount of potential energy is stored in HCIs. For example, a Xe^{44+} ion has a potential energy of about 51 keV.
- During ion–surface interactions, this potential energy is released within a few 10 fs over an area of about 100 nm^2, which leads to power densities of 10^{12} up to 10^{14} W cm^{-2}.
- Due to the high power density in the surface interaction area compared to low charged ions (LCIs), HCIs produce high amounts of secondary particles such as neutrals as well as secondary electrons and secondary ions.
- HCIs possess very strong static electric fields, reaching from 10^{14} up to 10^{16} V cm^{-1}.
- HCIs are characterized by a very effective stopping power (e.g. for Au^{69+}, 100 keV nm^{-1}).
- Due to their high ionic charge, HCIs can be accelerated very effectively ($\propto q$ for linear accelerators and $\propto q^2$ for circular accelerators; q denotes the ion charge state).
- Nowadays, HCIs can be produced in a compact laboratory set-up. Large accelerator structures are used if high HCI currents are necessary for a specific experiment but are not required for many applications.

These unique properties are the reason why the interest in HCIs is constantly growing and the number of applications increases. Figure 1 gives several examples for applications of HCIs in basic research as well as technology.

HCIs appear only in the plasma of fusion facilities, the corona of the Sun, at the border of black holes, and in similar exotic cosmic regions. The first publications on HCIs date back more than 80 years and the number of publications has increased continually. In the first classical papers Bowen and Millikan reported on the production of Se^{20+} ions in an arc discharge [1] in 1925 and Edlen explained the origin
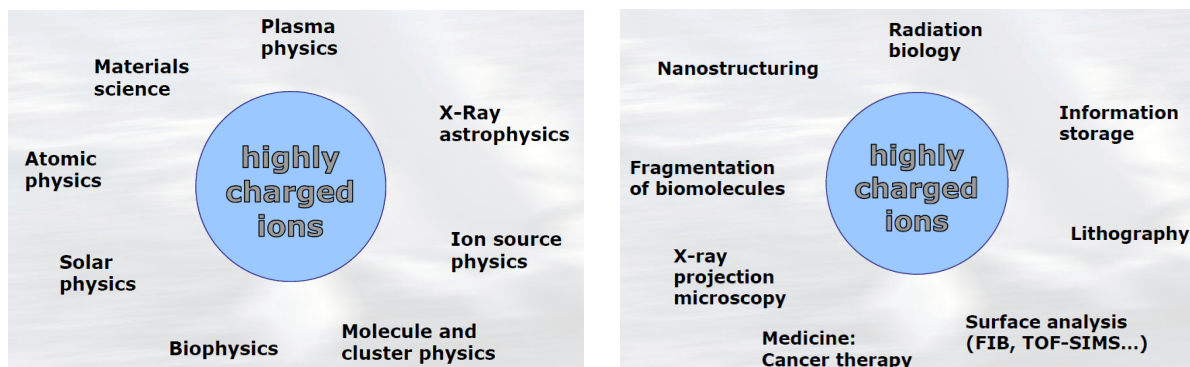
Fig. 1: Some applications of HCIs in basic research (left side) and possible applications in technology (right side)

of spectral lines in the corona of the Sun as emission lines from 10- to 15-fold ionized iron, calcium and nickel atoms in 1942 [2].

A classical approach to produce HCIs in the laboratory is the use of ion accelerators by stripping of energetic LCIs to all practically possible ion charge states. As a result of the stripping process, HCIs of high kinetic energy are produced, which must be decelerated in many cases for further use. Another way to access HCIs is the use of powerful ion sources such as the following:

– EBISs;
– electron cyclotron resonance (ECR) ion sources (ECRISs) (for basics see Ref. [3]); or
– laser ion sources (for basics see Ref. [4]).

This present chapter is about EBISs. For details on other kinds of ion sources, we refer to the citations above and the references therein. The aim of this work is to give a short up-to-date overview about the function and use of EBIS technology. More details can be found in the literature, e.g. in the book of Gillaspy [5] and the paper written by Currell [6]. More detailed information about the basic physics of HCIs can be found in the review by Gillaspy [7] and the book written by Beyer and Shevelko [8].

2 EBIS: the basic idea

2.1 The technical solution

EBIS/T ion sources have been known for more than 40 years and the technical design of these sources has been continually improved with increasing technical possibilities. The principle of operation of an EBIS is shown in Fig. 2.

The ion production in an EBIS is based on electron impact ionization in a high-density electron beam that is compressed by a strong magnetic field produced by magnetic coils. An electron gun with a cathode of high emissivity produces the electron beam. The ions that are produced by successive electron impact ionizations inside the electron beam are radially confined by the negative space charge of the electron beam, and the axial confinement of the ions is achieved by superposition of electrostatic potentials generated using a minimum of three collinear drift tubes. The higher potentials on the outer drift tubes create an axial electrostatic trap. Hence, the ionization time of the ions can be controlled by switching the axial trap potentials periodically on and off.

The magnetic field for the electron beam compression is generated by a special magnet system, which can consist of superconducting magnetic coils or permanent magnet rings. The electron beam is dumped in an electron beam collector where the electrons are separated from the extracted ions. Usually EBISs are equipped with one or more radial ports. This allows for spectrometry of electromagnetic radiation produced in the region of the ion trap during the ionization process.
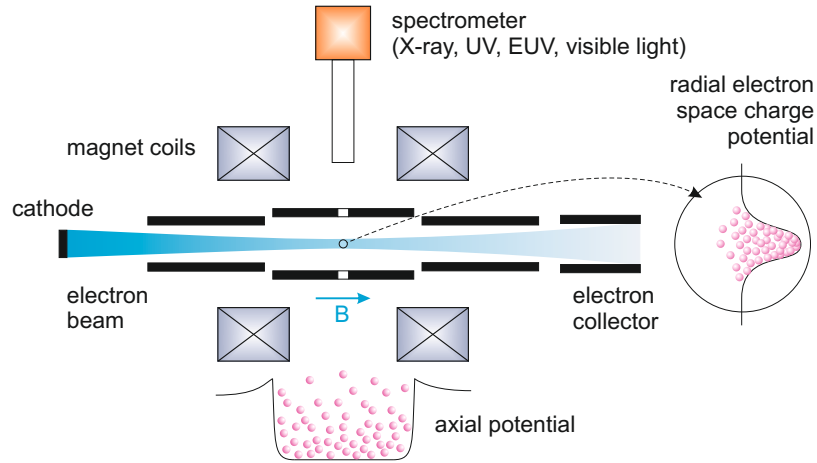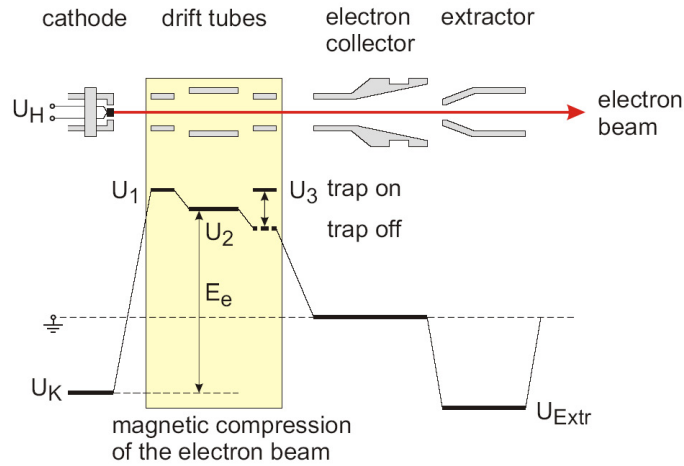
Fig. 2: Principle of operation of an EBIS

Fig. 3: Electrical scheme of EBIS operation: U_K, cathode potential; U_{Extr}, ion extraction potential; U_H, potential at the cathode heater; U_1, trap potential at the side of the electron gun; U_3, trap potential at the ion extraction side (switched for pulsed ion extraction); U_2, potential at the middle drift tube.

The electrical scheme of EBIS operation is shown in Fig. 3 for an EBIS with three drift tubes (solutions are also known with more drift tubes). The electron energy E_e in the centre of the drift tubes where the ions are produced and accumulated is

$$E_e = e(U_2 - U_K + U_e), \tag{1}$$

where U_e is the space-charge potential of the electron beam, which slightly decreases the final electron beam energy. The axial ion trap is controlled by switching the potential U_3 in the indicated manner. The chosen dynamics and height of the potential wall formed by the voltage U_3 allows the following three principal modes of source operation.

– *Permanently opened trap – transmission mode.* The trap is permanently open and ions are produced in the electron beam without axial trapping. This mode delivers high currents of the lowest charged ions with ion beam currents up to microamps.

– *Partially closed trap – leaky mode.* Selecting a low axial potential wall, a certain number of ions with adequate kinetic energy can overcome the potential wall and are extracted continuously. This mode delivers ions with preferentially low up to intermediate ion charge states and a small fraction of higher ion charge states, with ion beam currents up to nanoamps.

– *Periodically opened and closed trap – pulsed mode.* In this case the voltage U_3 is high enough to trap all ions axially. Periodic opening of the trap releases pulses of ions extracted with typical pulse widths in the order of some microseconds and allows the production of the highest currents of HCIs (up to microamps during the pulse).

Table 1 compares important practically realized parameters of cryogenic and room-temperature EBISs.

Table 1: Parameters of cryogenic and room-temperature EBISs.

Parameter	Cryogenic EBIS	Room-temperature EBIS
Magnetic system	superconducting coils (3–8 T) on axis	permanent magnets (SmCo, NdFeB) (250–600 mT) on axis
Electron beam currents	up to amps	≤ 200 mA
Electron beam energies	up to 200 keV	up to 30 keV
Electron beam densities	$j_e > 1000$ A cm^{-2}	$j_e < 500$ A cm^{-2}
Basic vacuum	up to 10^{-12} mbar	up to 10^{-10} mbar
Length of the ionization region	up to metres	≤ 6 cm
Ion charge states	highest ion charge states Xe^{54+}, U^{92+} at maximum	bare ions up to $Z = 28$, Kr^{34+}, Xe^{48+}, Au^{60+}, etc.
Set-up time	≥ 1 day	hours
Remarks	large devices liquid helium cooling latest developments: refrigerator cooling	compact transportable low initial and maintenance costs short set-up times

2.2 The history of EBISs: a short retrospect

EBIT/EBIS ion sources have now been available as reliable sources of HCIs for about 20 years. After the first demonstration of the working principle of an electron beam ion source (EBIS) in the pioneer works of Donets, Ovsyannikov and collaborators [9–11], the development of the first compact electron beam ion trap (EBIT) was reported by Levine *et al.* [12]. Starting from that date, many different EBIT/EBIS ion sources have been developed and put into operation at different places all over the world.

First of all, it seems to be necessary to clear up the terms 'EBIT' and 'EBIS'. Both terms can be found in the literature. The term EBIT stands for electron beam ion trap. Since all EBITs can in principle also work like an EBIS, it seems to be more common to speak about an EBIS unless the function as an ion trap is of interest, as is the case in spectroscopic studies on HCIs.

Making no claim to be complete, sources such as the LLNL EBIT, the NIST EBIT, the Tokyo EBIT, the Shanghai EBIT and the Heidelberg EBIT with their different modifications should be mentioned here. Furthermore, the first attempts to built a refrigerated (cryogenic closed cycle, no liquid helium) EBIT with a 2 cm ion trap using outer correction coils are known [13] and were realized with the Stockholm EBIT. Most of these EBITs are special constructions realized by several laboratories with the goal to perform specific investigations on highly charged ions.

Another line of development is the series of compact room-temperature EBIT/EBIS ion sources of the Dresden EBIT/EBIS family [14, 15]. They have a patented operation principle that allows the production of highly charged ions efficiently and with ion beam currents competitive with other known EBIT/EBIS solutions. Continuing this way a new refrigerated superconducting ion source, the Dresden EBIS-SC, was constructed and commissioned in 2010 [16]. In this context the basic idea was to build an ion source working with a liquid-helium-free refrigerator technique for cooling the superconductors that generate the strong magnetic field compressing the electron beam and to realize a very compact design of the source body. In spite of the compact ion source assembly, the system has proved successful for source operation with electron beams up to 700 mA.

An overview of EBIS installations in 2010 and earlier can be found in Ref. [17]. Nevertheless, the number of employed EBIS/EBIT is increasing permanently. In the last two years installations in Kielce and Krakow (both Poland), Huddersfield (Great Britain), Clemson (USA), Dresden-Rossendorf and Jena (both Germany) and Shanghai (China) have emerged.

Most of the EBISs of international reputation are special laboratory constructions, where each EBIS has its own particularities. Commercial versions of EBIT and EBIS devices are known only from two vendors:

- *Physics & Technology (Livermore, USA).* Offered is a so-called REBIT/S (Refrigerated Electron Beam Ion Trap/Source; for details see [13]).
- *Dreebit GmbH (Dresden, Germany).* Offered is a series of compact and efficient room-temperature EBIT and EBIS sources (Dresden EBIT, Dresden EBIS and Dresden EBIS-A) as well as a superconducting EBIS (Dresden EBIS-SC), using refrigerating technology for magnet cooling (for details see [15]).

3 EBISs: the basic physics

3.1 The ionization balance

The intended purpose of an EBIS is to produce highly charged ions. To produce HCIs a high-density electron beam acts as ionization medium. For neutrals and ions in the electron beam, the balance between

- charge generating processes and
- charge destructive processes

is of importance for reaching a certain ionization stage.

For ion production the dominant process is electron impact ionization. Therefore, only this process is considered at first. For the ion production in an EBIS we can write

$$
\begin{aligned}
\text{to } q=1 \qquad & \frac{\mathrm{d}n_0}{\mathrm{d}t} = -\lambda_1 n_0, \\
\vdots \qquad\qquad & \quad\vdots \qquad\qquad \vdots \\
\text{to } q \qquad & \frac{\mathrm{d}n_q}{\mathrm{d}t} = \underbrace{\lambda_q n_{q-1}}_{\text{ion production}} - \underbrace{\lambda_{q+1} n_q}_{\text{ion destruction}}, \\
\vdots \qquad\qquad & \quad\vdots \qquad\qquad \vdots \\
\text{to } Z \qquad & \frac{\mathrm{d}n_Z}{\mathrm{d}t} = \lambda_Z n_{Z-1},
\end{aligned}
\tag{2}
$$

where n_0 is the neutral particle density. For λ_q we have that

$$
\lambda_q = \sigma_q v_{\mathrm{e}} n_{\mathrm{e}} \qquad \text{(reaction rate)}, \tag{3}
$$

where λ_q has the dimension of s^{-1} and σ_q is the ionization cross-section, v_e the electron velocity and n_e the electron density.

If the ionization process starts only with neutral particles it yields

$$t = 0, \qquad n_0(0) = n_0^0, \qquad n_q(0) = 0.$$

This leads to the solution

$$
\begin{aligned}
n_0 &= n_0^0\, \mathrm{e}^{-\lambda_1 t}, \\[2mm]
n_1 &= \frac{n_0^0 \lambda_1}{\lambda_2 - \lambda_1}(\mathrm{e}^{-\lambda_1 t} - \mathrm{e}^{-\lambda_2 t}), \\[2mm]
n_2 &= n_0^0 \lambda_1 \lambda_2 \left(\frac{\mathrm{e}^{-\lambda_1 t}}{(\lambda_2 - \lambda_1)(\lambda_3 - \lambda_1)} + \frac{\mathrm{e}^{-\lambda_2 t}}{(\lambda_3 - \lambda_2)(\lambda_1 - \lambda_2)} + \frac{\mathrm{e}^{-\lambda_3 t}}{(\lambda_1 - \lambda_3)(\lambda_2 - \lambda_3)} \right), \\[2mm]
\vdots \quad & \quad \vdots \\[2mm]
n_q &= n_0^0 \prod_{l=1}^{q} \lambda_l \left(\sum_{j=1}^{q+1} \frac{\mathrm{e}^{-\lambda_j t}}{\prod_{k=1,\, k \neq q}^{q+1}(\lambda_k - \lambda_j)} \right).
\end{aligned}
\tag{4}
$$

In principle, Eq. (2) can also be integrated for other conditions, such as, for example, for $n_q(0) \neq 0$, for charge breeding processes or for external ion injection into an EBIS. With Eq. (3) the production rate of ions with individual ion charge states can be determined.

If we develop the exponents in Eq. (4) it yields

$$
\begin{aligned}
n_0 &= n_0^0(1 - \lambda_1 t), \\[2mm]
n_1 &= n_0^0 \lambda_1 t, \\[2mm]
n_2 &= n_0^0 \lambda_1 \lambda_2 \frac{t^2}{2}, \\[2mm]
\vdots \quad & \quad \vdots \\[2mm]
n_q &= n_0^0 \frac{t^q}{q!} \prod_{j=1}^{q} \lambda_j.
\end{aligned}
\tag{5}
$$

The characteristic time τ for ion production (ionization time) follows using

$$t_q = \frac{1}{\lambda_q} = \frac{1}{\sigma_q v_\mathrm{e} n_\mathrm{e}} \qquad \left(\frac{1}{\text{reaction rate}} \right),
\tag{6}$$

to give

$$
\begin{aligned}
\tau_1 &= t_1, \\[2mm]
\tau_2 &= t_1 + t_2, \\[2mm]
\vdots \quad & \quad \vdots \\[2mm]
\tau_q &= \sum_{k=1}^{q} t_q.
\end{aligned}
\tag{7}
$$

For estimating when a certain ionization stage reaches its maximum in the actual ion charge-state distribution, Eq. (7) can be used. Hence we write

$$j_\mathrm{e} \tau_q = \sum_{k=1}^{q} \frac{e}{\sigma_k} \qquad \text{(ionization factor)},
\tag{8}$$

with

$$j_\mathrm{e} = n_\mathrm{e} v_\mathrm{e}$$

as the electron beam density (A cm^{-2}). The ionization factor is a fundamental quantity that determines the ionization stage in an ion source.

The production of a mean ion charge state $\bar{q}$ is only possible if a certain $j\tau$ value (ionization factor) is reached. The following must hold:

$$j_\mathrm{e}\tau_q \geq \sum_{k=1}^{q} \frac{e}{\sigma_k}. \tag{9}$$

The precondition must be an electron energy E_e higher than the ionization potential I_q (ideally about $(2\text{--}3)\times I_q$).

The best values for the ionization factor and the electron beam energy under consideration of the excitation function of the electron-impact ionization cross-sections for selected elements are shown in Fig. 4. Thus producing high ionization stages requires

– a sufficient electron beam energy and
– a sufficiently high ionization factor.

Fig. 4: Interrelation between ionization factor and electron energy for the effective production of ions in different ion charge states (according to an idea of Prof. E. D. Donets (Dubna)).

In order to explain the role of electron binding energies, in Fig. 5 we show in more detail the electron binding energies of ions for different isoelectronic sequences as a function of the atomic number. Thereby it is considered that the ionization cross-section has its maximum at about 2.7 times the electron binding energy of the electron to be ionized.

In practice, processes such as

– charge exchange and
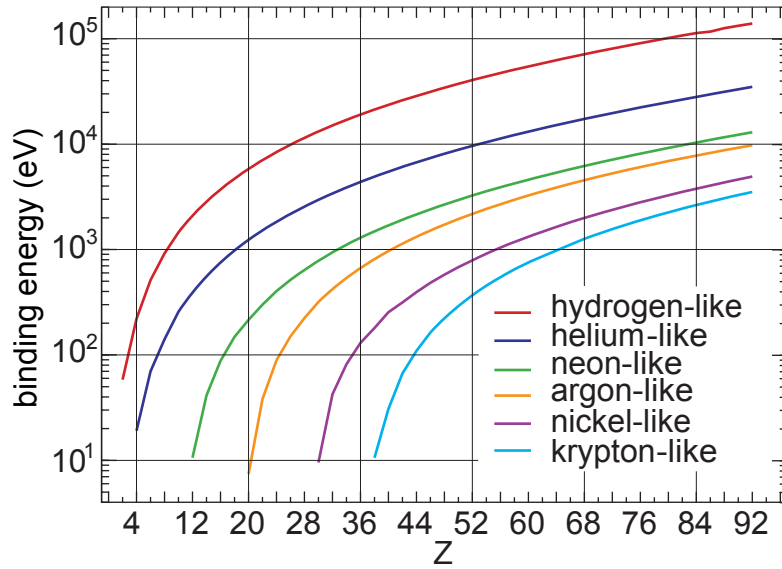– ion losses from the source

Fig. 5: Electron binding energies for the ion production of different isoelectronic sequences

can reduce the ionization power significantly. Of special importance in this case is the charge exchange with neutrals. The ionization factor as a function of the ionization time and the electron energy for selected isoelectronic sequences is given in Table 2 (according to Ref. [18]).

Figure 6 shows this behaviour for xenon ions. The ionization factor for the production of a certain ion charge state is minimal at 2.7 times the electron binding energy and increases again at higher electron energies. To produce the highest ionization charge states, ionization factors many orders of magnitude higher than those ones for low charged ions must be reached. It should be noted again that the issues discussed are only valid under the idealized condition that only electron impact ionization takes place.
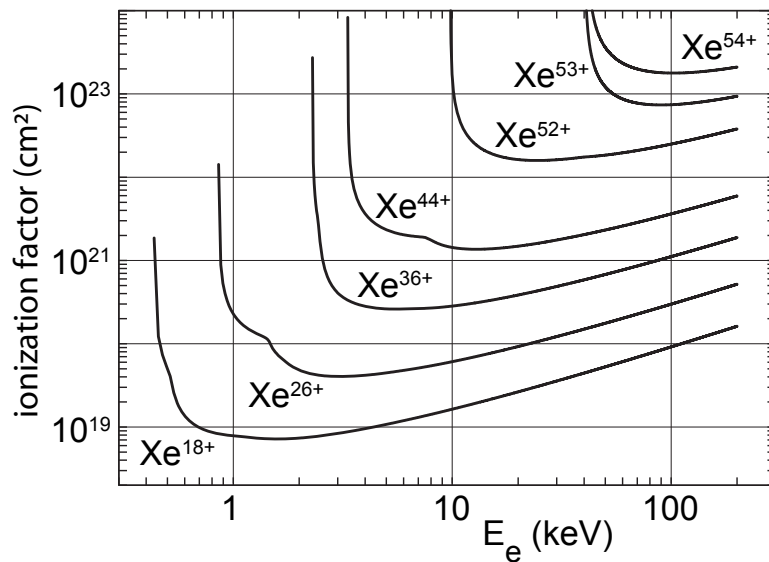

Fig. 6: Ionization factors for the production of individual xenon ionization charge states

Table 2: Ideal production conditions for ions of different isoelectronic sequences. Given are the ionization factor $j_e\tau$ (e^- cm^{-2}), the optimal electron beam energy (keV) and the required ionization time (ms or s) for an assumed ionization factor of $j_e\tau = 3 \times 10^{22}$ e^- cm^{-2}.

Sequence	Neon $Z = 10$	Argon $Z = 18$	Krypton $Z = 36$	Xenon $Z = 54$	Gold $Z = 79$	Uranium $Z = 92$
Atom fully ionized	Ne^{10+} 2×10^{21} 3 7 ms	Ar^{18+} 2×10^{21} 9 67 ms	Kr^{36+} 3×10^{22} 40 1 s	Xe^{54+} 2×10^{23} 80 7 s	Au^{79+} 6×10^{23} 180 20 s	U^{92+} $2 \times 10^{24+}$ 300 67 s
Helium-like	Ne^{8+} 8×10^{18} 0.6 0.3 ms	Ar^{16+} 1×10^{20} 2 3 ms	Kr^{34+} 2×10^{21} 7 67 ms	Xe^{52+} 2×10^{22} 20 0.7 s	Au^{77+} 6×10^{22} 45 2 s	U^{90+} 2×10^{23} 70 7 s
Neon-like		Ar^{8+} 3×10^{18} 0.3 0.1 ms	Kr^{28+} 3×10^{20} 4 10 ms	Xe^{44+} 2×10^{21} 8 67 ms	Au^{69+} 6×10^{21} 17 200 ms	U^{82+} 3×10^{22} 30 1 s
Argon-like			Kr^{18+} 1×10^{19} 1.5 0.3 ms	Xe^{36+} 2×10^{20} 5 7 ms	Au^{61+} 1×10^{21} 12 33 ms	U^{74+} 5×10^{21} 20 167 ms
Krypton-like				Xe^{18+} 6×10^{18} 1 0.4 ms	Au^{43+} 1×10^{20} 4 3 ms	U^{56+} 7×10^{20} 7 23 ms
Xenon-like					Au^{25+} 2×10^{19} 1.5 0.7 ms	U^{38+} 7×10^{19} 4 2 ms

3.2 Atomic physics for ion production

3.2.1 Overview

The following are the atomic processes contributing to ion production;

1. electron impact ionization,
2. charge exchange,
3. recombination,
4. three-body recombination,
5. dielectronic recombination,
6. photoionization,
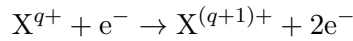7. vacancy cascades and
8. electron shake-off processes.

Later on we will discuss these further processes that are important for ion losses and the energy balance in EBISs:

- – ion heating by elastic electron collisions,
- – ion–ion energy exchange,
- – ion confinement and
- – ion losses from the trap.

In the following we will discuss the most important processes in more detail. For the basic atomic processes, some useful estimation formulas are given. Nevertheless, we note that these formulas do not completely substitute more precise quantum-mechanical calculations for individual processes.

3.2.2 Direct Coulomb ionization

In simple cases, the cross-sections for single electron impact ionization

$$X^{q+} + e^- \rightarrow X^{(q+1)+} + 2e^-$$

can be estimated for different subshells j by the Lotz formula [19]

$$\sigma_{qj} = a_{qj} g_{qj} \frac{\ln(E_e/I_{qj})}{E_e I_{qj}} \left\{ 1 - b_{qj} \exp\left[-c_{qj} \left(\frac{E_e}{I_{qj}} - 1 \right) \right] \right\}. \tag{10}$$

For all ionization processes, the electron energy E_e must be greater than the related ionization potential I_{qj}, otherwise the ionization cross-section is equal to zero. The quantities a_{qj}, b_{qj} and c_{qj} are tabulated constants. For highly charged ions, they are given by

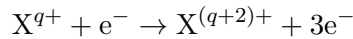$$a_{qj} = 4.5 \times 10^{-14} \text{ cm}^2 \text{ eV}^2$$

and

$$b_{qj} = c_{qj} = 0,$$

with g_{qj} as the occupation number of the subshell j of an ion in the charge state q. The quantity I_{qj} is the ionization potential for the ionization of the subshell j. The total ionization cross-section results as a sum over all occupied subshells:

$$\sigma_q(E_e) = \sum_q \sigma_{qj}(E_e). \tag{11}$$

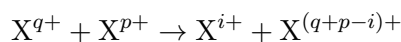As an example, the electron impact ionization cross-sections for argon ions are shown in Fig. 7 [20].

We will not go into the details for the double ionization process

$$X^{q+} + e^- \rightarrow X^{(q+2)+} + 3e^-$$

but we refer the reader to the estimation formula from Mueller and Frodel [21], which was derived from experimental data. As a rule double ionization cross-sections for most species are about one order of magnitude or more lower than cross-sections for single ionization cross-sections.

3.2.3 Charge exchange

The charge exchange between ions can be written as

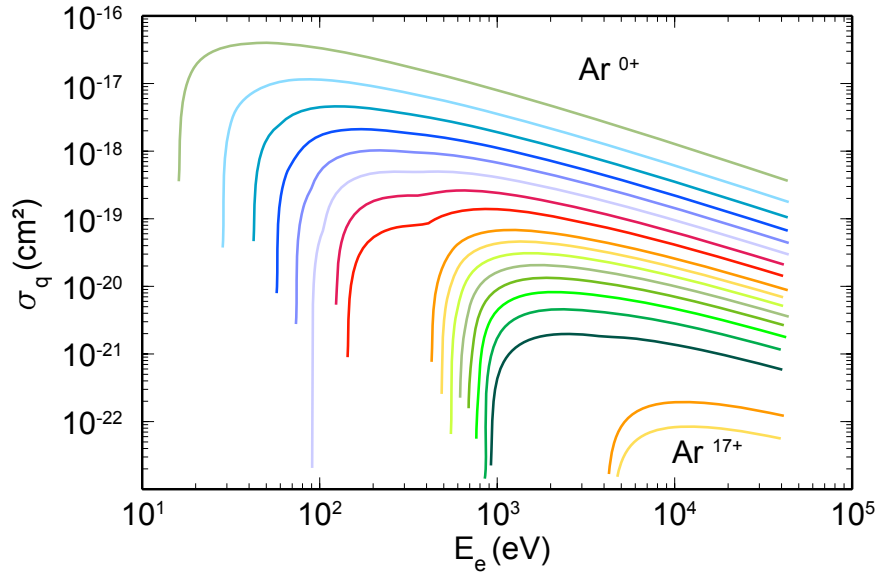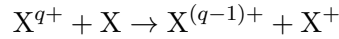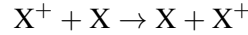$$X^{q+} + X^{p+} \rightarrow X^{i+} + X^{(q+p-i)+}$$

Fig. 7: Single electron impact ionization cross-sections as a function of the electron energy (according to Ref. [20])

and correspondingly for the charge exchange with a neutral atom

$$X^{q+} + X \rightarrow X^{(q-1)+} + X^+$$

Owing to the fact that

$$X^+ + X \rightarrow X + X^+$$
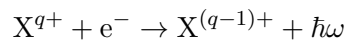
charge exchange does not play a role for singly charged ions.

Of special importance in this case is the charge exchange of ions with neutrals due to the very high cross-sections. This circumstance is important for EBIS operation and can limit the reachable ionization stages in the electron beam. For collision energies below 25 keV/u, charge exchange can be estimated by the formula from Mueller and Salzborn [22]

$$\sigma_{q \rightarrow q-1} \, (\text{cm}^2) \approx (1.43 \pm 0.76) \times 10^{-12} \, q^{1.17} \, [I_q \, (\text{eV})]^{-2.76} \tag{12}$$

and is of the order of 10^{-14}–10^{-15} cm^{-2}. As a rule, charge exchange is the dominant loss mechanism for highly charged ions and is especially important if the gas pressure in the ion source is relatively high. As we can see from Eq. (12), the cross-section is independent of the energy of the projectiles. In Fig. 8 cross-sections for single and double charge exchange are given for xenon ions.

3.2.4 *Radiative recombination*

The scheme for radiative recombination (RR)

$$X^{q+} + e^- \rightarrow X^{(q-1)+} + \hbar\omega$$

is shown in Fig. 9.

The cross-section for charge exchange processes can be estimated by the formula from Kim and Pratt [24]

$$\sigma_q^{\text{RR}}(E_\text{e}) = \frac{8\pi}{3\sqrt{3}} \alpha \lambda_\text{e}^2 \chi_q(E_\text{e}) \ln\left(1 + \frac{\chi_q(E_\text{e})}{2\hat{n}}\right), \tag{13}$$

with

$$\chi_q(E_\mathrm{e}) = (Z + q)^2 \frac{I_\mathrm{H}}{4E_\mathrm{e}}$$

and

$$\hat{n} = n + (1 - W_n) - 0.3.$$

Here n is the main quantum number of the valence shell, W_n is ratio of the number of unoccupied states to the total number of states in the valence shell, $\lambda_\mathrm{e} = 3.861 \times 10^{-11}$ cm (electronic Compton wavelength) and $I_\mathrm{H} = 13.6$ eV. As an example we show the cross-sections for radiative recombination on xenon ions as a function of the electron energy in Fig. 10.

Fig. 8: Charge exchange cross-sections for single charge exchange with Xe$^{(0,1,2)}$ ions as well as for the double charge exchange with xenon neutrals (after Ref. [23]).

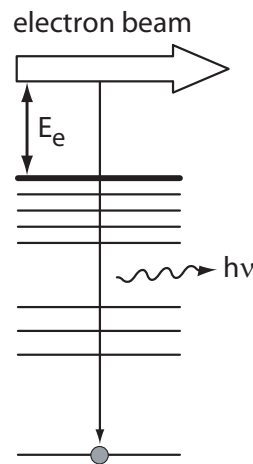**Fig. 9:** Scheme of the radiative recombination process. The energy $\hbar\omega$ of the emitted photon is calculated as $\hbar\omega = E_\mathrm{e} - E_\mathrm{B}$, where E_B is the electron binding energy.
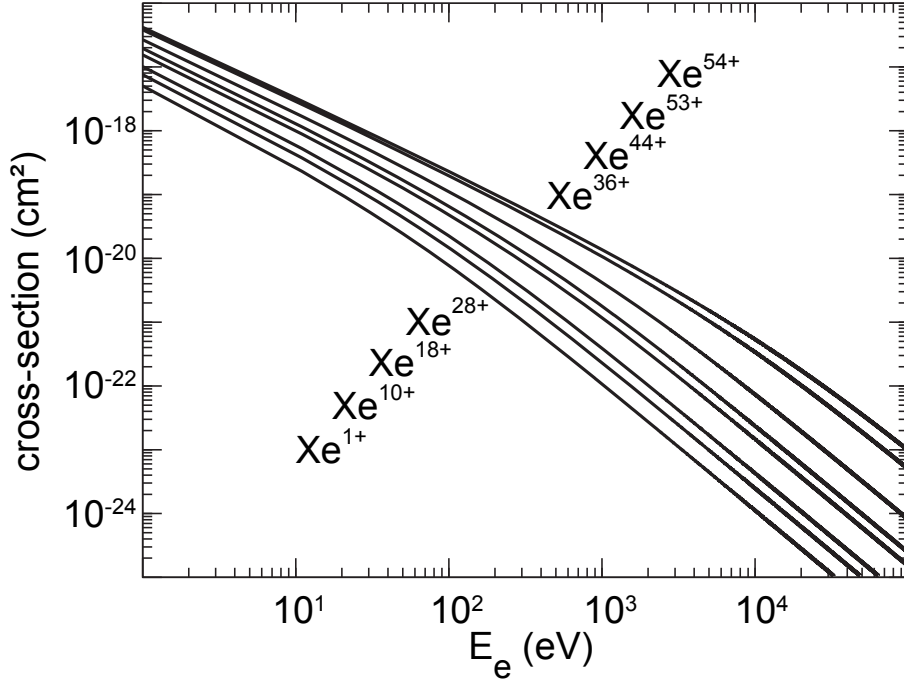
Fig. 10: Cross-sections for the radiative recombination on xenon ions (according to Ref. [23])

Since RR processes counteract the ionization for each element and ion charge state, there exists a characteristic electron energy at which the ionization rate is equal to the RR rate. This behaviour is discussed in more detail in Ref. [25].

3.2.5   *Further processes*

Besides the main processes discussed above, in special cases some further contributions from

  – dielectronic recombination (DR),
  – three-body recombination,
  – vacancy cascades and
  – photoionization

are of interest, but they will not be discussed here.

3.3   Balance equation for the ion charge-state distribution

The number of ions with charge q produced from ions with charge $(q-1)$ and ionized further to the charge state $(q+1)$ can be described by a balance equation for successive electron impact ionization and competing processes:

$$
\begin{aligned}
\frac{\mathrm{d}n_q}{\mathrm{d}t} \;=\; & R^{\mathrm{ion}}_{q-1 \to q} - R^{\mathrm{ion}}_{q \to q+1} + R^{\mathrm{RR}}_{q+1 \to q} - R^{\mathrm{RR}}_{q \to q-1} \\
& + R^{\mathrm{exch}}_{q+1 \to q} - R^{\mathrm{exch}}_{q \to q-1} - R^{\mathrm{ax,esc}}_{q} - R^{\mathrm{rad,esc}}_{q} + R^{\mathrm{source}},
\end{aligned}
\tag{14}
$$

with ionization terms R^{ion}, radiative recombination terms R^{RR}, charge exchange terms R^{exch}, axial ion loss terms $R^{\mathrm{ax,esc}}$, radial ion loss terms $R^{\mathrm{rad,esc}}$ and particle source term R^{source}.

If the ionization process occurs in single-step processes and if we neglect the axial loss (which is a good approximation for appropriate field configurations) this yields

$$
\begin{aligned}
\frac{\mathrm{d}n_0}{\mathrm{d}t} &= \underbrace{-n_0\lambda_{0,1}}_{\text{ionization}} + \underbrace{n_1\lambda_{1,0}}_{\text{charge exchange}}, \\
\frac{\mathrm{d}n_1}{\mathrm{d}t} &= n_0\lambda_{0,1} - n_1(\lambda_{1,2} + \lambda_{1,0}) + n_2\lambda_{2,1} - \left[\frac{\mathrm{d}n_1}{\mathrm{d}t}\right]^{\text{rad,esc}}, \\
&\ \vdots \\
\frac{\mathrm{d}n_q}{\mathrm{d}t} &= n_{q-1}\lambda_{q-1,q} - n_q(\lambda_{q,q+1} + \lambda_{q,q-1}) + n_{q+1}\lambda_{q+1,q} - \left[\frac{\mathrm{d}n_q}{\mathrm{d}t}\right]^{\text{rad,esc}}, \\
\frac{\mathrm{d}n_z}{\mathrm{d}t} &= n_{Z-1}\lambda_{Z-1,Z} - n_Z\lambda_{Z,Z-1} - \left[\frac{\mathrm{d}n_Z}{\mathrm{d}t}\right]^{\text{rad,esc}}.
\end{aligned}
\tag{15}
$$

Here $n_0, \ldots, n_Z$ are the densities for neutrals and ions of the charge state q. Further we have the ionization coefficients $\lambda_{q,q+1}$ and the recombination and charge exchange coefficients $\lambda_{q,q-1}$. Details about the corresponding terms, the influence on the development of the individual ion densities, the development of the energy densities and ion evaporation of ions from the ionization volume can be found, for example, in Refs. [26] and [27].

In Fig. 11, as a typical example we show the evolution of xenon ion charge states in the electron beam of a Dresden EBIT as it follows from equation system (14).
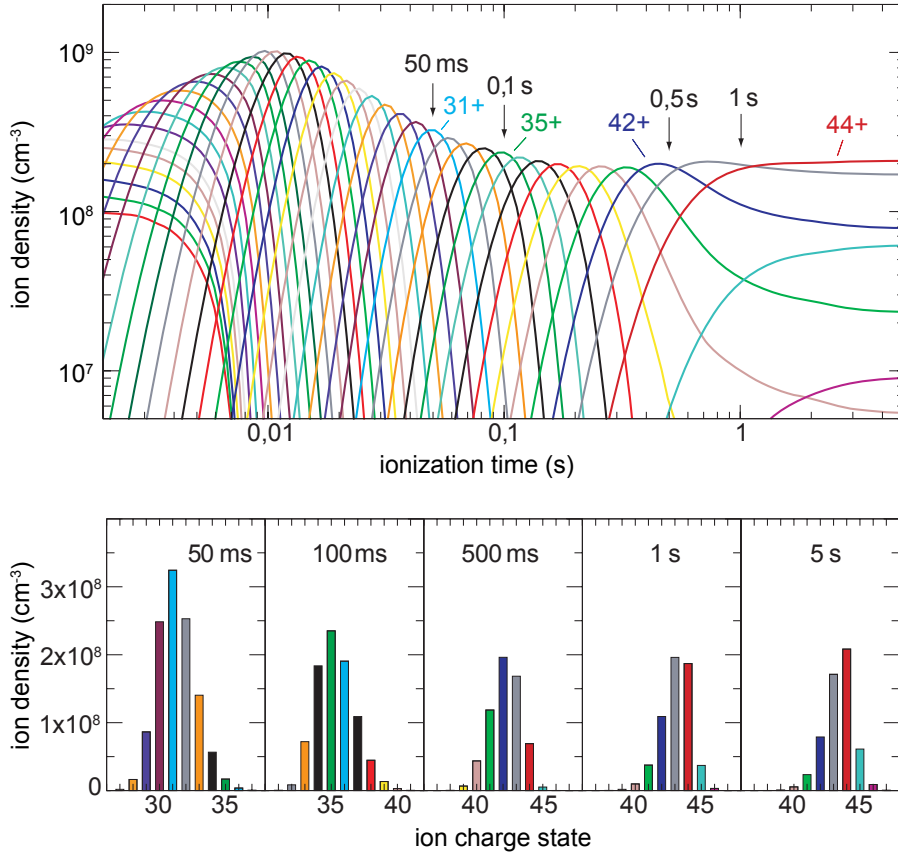

Fig. 11: Evolution of the ionization of xenon ions in a Dresden EBIT at $E_e = 15$ keV, $I_e = 40$ mA and $p = 2 \times 10^{-9}$ mbar.

3.4 Ion source physics: selected topics

Owing to the restricted scope of this chapter, only some information about the important (but not complete) details of EBISs are given. For more detailed studies, please refer to the corresponding literature. For reasons of simplicity and copyright, in the following the author will give examples of results from EBISs of the Dresden EBIS type.

3.4.1 Electrical trap capacity

The ion trapping in an EBIS (see Fig. 12) occurs

- in the axial direction by electrostatic potentials and
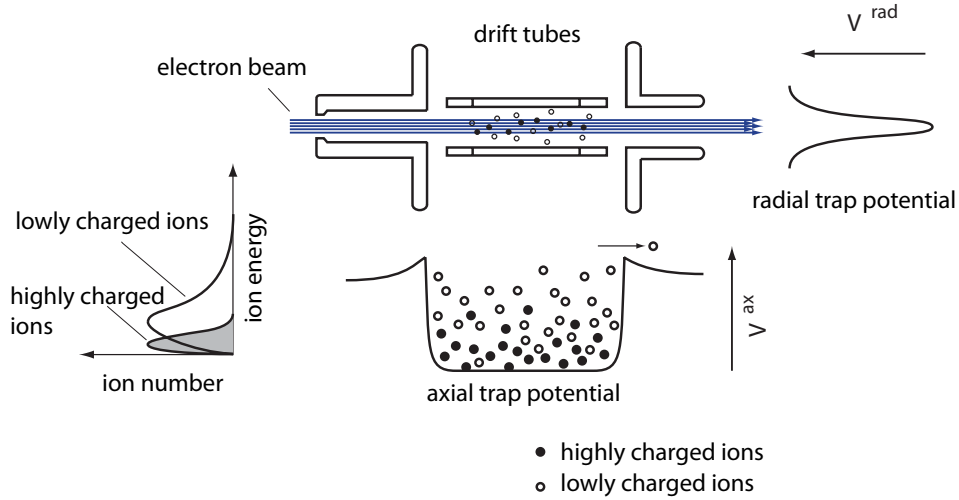- in the radial direction by the space-charge potential of the electron beam.

Fig. 12: Axial and radial potentials in an EBIT. Owing to the effective trap height according to $V_{\rm b} \times q$, highly charged ions are trapped more strongly than low charged ones. The energy exchange between the ions leads to an equilibrium distribution of the ion energy.

The total number of ions that can be stored in an EBIS is limited by the electrical trap capacity $C_{\rm el}$. For an estimation of $C_{\rm el}$, we assume a homogeneous electron beam that passes through an ion trap of length L with the electron beam current $I_{\rm e}$ and electron energy $E_{\rm e}$. Then the number of negative charges in the beam volume is a measure for the trap capacity $C_{\rm el}$. With

$$I_{\rm e} = \frac{{\rm d}Q}{{\rm d}t}, \qquad v_{\rm e} = \frac{{\rm d}x}{{\rm d}t}, \qquad v_{\rm e} = \sqrt{\frac{2E_{\rm e}}{m_{\rm e}}},$$

we have

$$\Delta Q = \frac{I_{\rm e}\Delta x}{v_{\rm e}} = \frac{I_{\rm e}L}{\sqrt{2E_{\rm e}/m_{\rm e}}}$$

and for the trap capacity

$$C_{\rm el} = 1.05 \times 10^{13} \frac{I_{\rm e}\,({\rm A})\,L\,({\rm m})}{\sqrt{E_{\rm e}\,({\rm eV})}}. \tag{16}$$

In order to estimate the useable trap capacity, in practice we must supplement Eq. (16) to

$$C_{\rm el} = 1.05 \times 10^{13} \frac{I_{\rm e}\,({\rm A})\,L\,({\rm m})}{\sqrt{E_{\rm e}\,({\rm eV})}}\,\alpha f, \tag{17}$$

with α the ratio of ions with a certain ion charge state in the ion charge-state distribution and f the charge compensation of the electron beam.

3.4.2 Boltzmann distribution of the ion energy

In the source volume ion–ion collisions lead very rapidly (in about milliseconds) to a Boltzmann distribution of the ion energy

$$f(E_i) = \frac{2}{\sqrt{\pi}\, kT_i} \sqrt{\frac{E_i}{kT_i}} \exp\left(-\frac{E_i}{kT_i}\right). \tag{18}$$

The formation of a Boltzmann energy distribution has consequences for the whole ion trap process:

- *Permanent ion losses.* At a certain mean ion energy, ions always exist with an energy greater than a critical energy

$$E_{cr} = qU_b, \tag{19}$$

  and can leave the trap with the barrier U_b. This means that we have a constant ion loss from the trap. The ion loss ratio can be derived by integrating the distribution function. The behaviour of ions in the trap can be described by the non-stationary Boltzmann equation in a self-consistent model considering ionization and energy exchange processes.

- *Evaporative cooling* of multiply charged ions by light LCIs. Elastic collisions between ions with different charge states and masses lead to an equilibrium energy distribution for each ion sort. Thereby the critical energy for leaving the ion trap for LCIs is lower than for highly charged ions, i.e. the ion lifetime in the ion trap is lower for LCIs. LCIs leave the beam first, i.e. they evaporate and transport the energy transmitted from the highly charged ions to lower charged ones out of the ionization volume. As a result of the process, the mean temperature of the highly charged ions decreases and ion losses of these ions are reduced.

3.4.3 Radial trap potential

For simplicity, we consider an ion trap with a radial symmetric electron beam the electron density of which is homogeneously distributed over the radius r_e of the electron beam. Using Gauss's theorem the radial trap potential has the shape

$$V_e(r) = \begin{cases} \dfrac{U_e r^2}{r_e^2} & \text{for } r < r_e, \\[2ex] U_e\left(2\ln\dfrac{r}{r_e} + 1\right) & \text{for } r > r_e. \end{cases} \tag{20}$$

Here we have

$$U_e = \frac{I_e}{4\pi\varepsilon_0 v_e} = \frac{1}{4\pi\varepsilon_0} \sqrt{\frac{m_e}{2}} \frac{I_e}{\sqrt{E_e}}. \tag{21}$$

We can estimate U_e with

$$U_e\,(\text{V}) = \frac{30 I\,(\text{A})}{\sqrt{1 - \left(\dfrac{E_e\,(\text{keV})}{511} + 1\right)^{-2}}}. \tag{22}$$

As an example the radial trap potential in Fig. 13 is shown for a typical operation regime of a Dresden EBIT.

The ion confinement is additionally influenced by the magnetic field enclosing the electron beam, so that we finally have an effective radial potential of

$$V_e^{\text{eff}}(r) = V_e(r) + \frac{eq_i B^2 r^2}{8 m_i}, \tag{23}$$

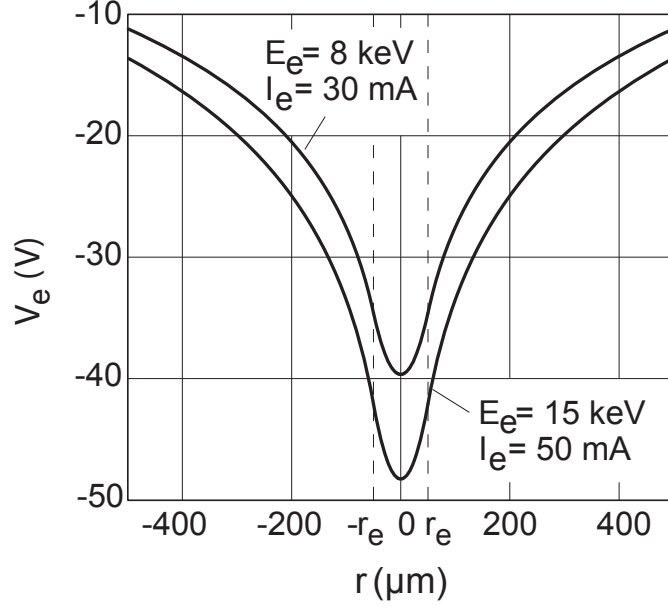with R the drift tube radius.

Fig. 13: Radial trap potential of a Dresden EBIT for two different electron beam currents

3.4.4 Ion heating and energy balance

Ions are heated in the electron beam by elastic Coulomb collisions and by microwave instabilities. If instabilities do not appear (huge Debye lengths), the main heating processes are elastic electron–ion collisions.

3.4.4.1 Elastic electron–ion collisions

Ion heating by elastic electron collisions can be described by

$$\left[\frac{\mathrm{d}E_\mathrm{i}}{\mathrm{d}t}\right]^{\mathrm{heat}} = (n_\mathrm{i}\sigma_\mathrm{i} v_\mathrm{e})\left(2\frac{m_\mathrm{e}}{m_\mathrm{i}}E_\mathrm{e}\right) = 2\frac{m_\mathrm{e}}{m_\mathrm{i}}E_\mathrm{e} f_\mathrm{ei}, \tag{24}$$

with

$$t_\mathrm{ei} = f_\mathrm{ei}^{-1} = \frac{1}{n_\mathrm{i}\langle v_\mathrm{e}\sigma_\mathrm{i}\rangle}$$

and σ_i the Coulomb collision cross-section

$$\sigma_\mathrm{i} = \frac{1}{(4\pi\varepsilon_0)^2}4\pi\left(\frac{q_\mathrm{i}e^2}{m_\mathrm{e}}\right)^2\frac{\ln\Lambda_\mathrm{ei}}{v_\mathrm{e}^4}.$$

The Coulomb logarithm for electron–ion collisions $\ln\Lambda_\mathrm{ei}$ has the shape

$$\ln\Lambda_\mathrm{ei} = \begin{cases} 23 - \ln\dfrac{q_\mathrm{i}\sqrt{n_\mathrm{e}}}{(kT_\mathrm{e})^{3/2}} & \text{for } q_\mathrm{i}^2\times 10\,\mathrm{eV} > kT_\mathrm{e} > \dfrac{m_\mathrm{e}}{m_\mathrm{i}}kT_\mathrm{i}, \\[2ex] 24 - \ln\dfrac{\sqrt{n_\mathrm{e}}}{(kT_\mathrm{e})} & \text{for } kT_\mathrm{e} > q_\mathrm{i}^2\times 10\,\mathrm{eV} > \dfrac{m_\mathrm{e}}{m_\mathrm{i}}kT_\mathrm{i}, \\[2ex] 30 - \ln\dfrac{q_\mathrm{i}^2\sqrt{n_\mathrm{e}}}{(kT_\mathrm{i})^{3/2}A_\mathrm{i}} & \text{for } kT_\mathrm{e} < \dfrac{m_\mathrm{e}}{m_\mathrm{i}}q_\mathrm{i}kT_\mathrm{i}, \end{cases} \tag{25}$$

with kT the energy (eV), n the density (cm^{-3}), A_i the atomic mass and k the Boltzmann constant. Energy transfer by Coulomb collisions then occurs with a rate

$$\left[\frac{\mathrm{d}(n_\mathrm{i}kT_\mathrm{i})}{\mathrm{d}t}\right]^{\mathrm{heat}} \approx \left(-\frac{\mathrm{d}E_\mathrm{e}}{\mathrm{d}t}\right)n_\mathrm{e}. \tag{26}$$

3.4.4.2 Elastic ion–ion collisions

Energy transfer between ions occurs by elastic ion–ion collisions. In these collisions energetic ('hot') ions are cooled by colder ions. If we assume a Boltzmann distribution of the ion energy, the cooling process can be characterized by

$$\left[\frac{\mathrm{d}E}{\mathrm{d}t}\right]^{\mathrm{exch}} = 2\nu_{ij}n_i\frac{m_i}{m_j}\frac{kT_j - kT_i}{\left(1 + \dfrac{m_iT_j}{m_jT_i}\right)^{3/2}}. \tag{27}$$

Here the ν_{ij} are Coulomb collision rates between the ions

$$\nu_{ij} = \frac{1}{(4\pi\varepsilon_0)^2}\frac{4\sqrt{2\pi}}{3}n_j\left(\frac{q_iq_je^2}{m_i}\right)^2\left(\frac{m_i}{kT_i}\right)^{3/2}\ln\Lambda_{ij}, \tag{28}$$

with Λ_{ij} as the Coulomb logarithm for ion–ion collisions

$$\ln\Lambda_{ij} = \ln\Lambda_{ji} = 23 - \ln\left[\frac{q_iq_j(m_i + m_j)}{m_iT_j + m_jT_i}\left(\frac{n_iq_i^2}{T_i} + \frac{n_jq_j^2}{T_j}\right)^{1/2}\right]. \tag{29}$$

The energy transfer by ion–ion collisions is applied for evaporative cooling where low charged ions cool down more highly charged ions. The the rest gas in the source acts as the source for the LCIs. Because ion–ion collisions occur very efficiently, the ions tend to thermal equilibrium. The energy that the ions have on leaving the ion trap is then proportional to the ion charge state. It is important to mention that there exists an upper limit for the neutral gas density because otherwise the number of highly charged ions will be reduced dramatically by charge exchange processes.

The energy that is transferred out of the ion source by the evaporation process can be described by the cooling rate

$$\frac{\mathrm{d}E_0}{\mathrm{d}t}\left(\frac{\mathrm{eV}}{\mathrm{s\,cm^3}}\right) = \frac{\mathrm{d}n_{\mathrm{LCI}}\,(\mathrm{cm^{-3}})}{\mathrm{d}t}U_{\mathrm{b}}\,(\mathrm{V})\,q_{\mathrm{LCI}}, \tag{30}$$

with n_{LCI} the equilibrium density of the LCIs and q_{LCI} the ion charge state of the LCIs.

3.4.5 Electron beam: equation of motion and beam radius

The equation of motion for the electron beam in the paraxial approximation can be written as

$$\frac{\mathrm{d}^2r}{\mathrm{d}t^2} = \frac{eI_\mathrm{e}}{2\pi\varepsilon_0 v_z r m_\mathrm{e}} + \frac{e^2}{4m_\mathrm{e}^2}\left(\frac{B_\mathrm{c}^2r_\mathrm{c}^4}{r^3} - B_z^2r\right), \tag{31}$$

with B_c the B field at the cathode, B_z the axial magnetic field, r_c the cathode radius, I_e the electron beam current and v_z the axial electron velocity.

If we assume $B_\mathrm{c} = 0$ then there exists a stationary solution of Eq. (31). The solution corresponds to an equilibrium flow of electrons with constant radius, the so-called Brillouin flow (index 'B'). For a Brillouin flow, all electrons have a constant distance to the beam centre. Thereby the Lorentz force caused by the magnetic field is compensated by the space charge and the centrifugal force of the rotating electrons.

If we consider more realistic assumptions, such as

- a magnetic field at the cathode,
- thermal effects at the cathode due to filament heating up to the temperature T_c and
- interactions between the electrons,

then this leads to a corrected electron beam radius (smaller than r_B) as described by Herrmann [28]. According to Herrmann's theory the electron beam radius enclosing 80% of the beam is calculated [29] to be

$$r_e = r(0)\sqrt{\left(1 - \frac{r_0}{r(0)}\right)^2 + \frac{2}{1 + (B_c^2 r_c^4/B_z^2 r_0^4)}\left(\frac{v_e \tan\gamma}{(e/m_e)B_z\gamma}\right)}, \qquad (32)$$

and

$$r_0 = r_B\left\{\frac{1}{2} + \frac{1}{2}\left[1 + 4\left(\frac{8kT_c r_c^2 m_e}{e^2 B_z^2 r_B^4} + \frac{B_c^2 r_c^4}{B_z^2 r_B^4}\right)\right]^{1/2}\right\}^{1/2}, \qquad (33)$$

with $r(0)$ the beam radius at the cathode and γ the angle deviation from the source axis.

Generally, the electron beam diameter of an EBIT depends on the actual technical solution. Typical diameters are of the order of 40 µm up to about 200 µm. A classical method to measure the electron beam diameter in an EBIS is shown in Fig. 14 and is discussed in more detail in Ref. [30]. The idea is to measure the X-rays emitted from ions in the electron beam that are ionized or excited by electron impact. Through an aperture the X-rays are detected on a charge-coupled device (CCD) chip and the evaluation of the measured intensity distributions allows the electron beam diameter to be determined.

Fig. 14: CCD chip imaging of X-rays emitted from the electron beam (after Ref. [30]). Here $I(x)$ is the X-ray intensity distribution from the electron beam, and $I(x')$ is the intensity distribution on the CCD.

4 Ion extraction from EBISs

4.1 Basic ion extraction techniques

As mentioned before, EBISs allow for production of ion beams in DC as well as pulsed mode. In the following, we will discuss and characterize some basic features of EBIS ion extraction. If ions from an EBIS are applied in different experiments, a basic problem is the separation of an individual ion charge state from the extracted ions, which primarily contain a spectrum of individual ion charge states. Generally, the ion charge-state separation is realized by

– magnetic dipole analyzer or
– Wien filters.

4.2 Ion beam separation using an analysing magnet

A typical experimental set-up for experiments with extracted ions and magnetic analysis of the ion charge states is shown in Fig. 15. The facility shown was designed for experiments with highly charged ions for ion–solid interactions, atomic physics, biophysics, plasma physics, materials analysis, solid-state physics, etc. The ion source as well as the ion beamline can be insulated from ground potential. Thus ions with a wide range of kinetic energies (decelerated as well as accelerated) can be used for experiments in the target chamber of the facility, which can be subdivided into four functional units, the ion source (e.g. Dresden EBIS-A), the first and second beamline segments, and the target chamber.

Fig. 15: Footprint of an ion beam facility featuring a Dresden EBIS-A including a 90° bending magnet for mass-to-charge ratio separation of the ion beam extracted from the EBIS.

An einzel lens and an x–y deflector as well as an aperture, a four-jaw slit system and a Faraday cup are integrated in the first beamline segment. The einzel lens and the x–y deflector are used to focus, deflect and align the ion beam. An aperture with variable diameters can be used, reducing the phase space of the ion beam and therefore improving the beam quality at the expense of beam intensity. A Faraday cup is used for detecting and measuring the ion beam current. It is mounted onto a translational feedthrough directly behind the four-jaw slit system, which is positioned in the focal point of the dipole magnet. Thus the determination of the beam position as well as the beam size is possible.

The ion beam extracted from the ion source can consist of ions of various elements and ion charge states. Thus a dipole magnet separates the ions according to their momentum in the second beamline segment. The momentum of the ion depends on the charge state and the mass of the ion. Hence ions with a certain charge-to-mass ratio can be selected.

The momentum-separated ions are aligned and deflected with a second x–y deflector positioned behind the dipole magnet. A second Faraday cup mounted in the focal point downstream of the dipole magnet ensures detection and current measurement of the ion beam using an electrometer.

The last functional unit of the facility consists of a deceleration lens and the target chamber. The ions are focused into the target chamber by the deceleration lens system. In principle, it is possible to decelerate the ions down to a few electronvolts as well as to accelerate them up to some tens of keV (40 keV) per charge state. In the example shown, the target chamber has two stages, an upper one for target irradiation experiments and a lower one for target preparation and target transfer. The upper stage is mounted onto the deceleration lens system. The target can be rotated (360°) and transferred via a sample holder mounted to a four-axes manipulator. The target can be heated by resistance heating as well as electron bombardment and cooled down via liquid nitrogen. With a 'wobble stick' a further target manipulation inside the target chamber is possible. For measuring the beam intensity in the target chamber, a third Faraday cup is mounted onto the four-axes manipulator below the sample holder. A large number of vacuum ports allow the installation of various devices for experiments.

To characterize ion extraction spectra with an analysing magnet, some examples for ion extraction spectra are given as they can be expected for EBISs. Figure 16 shows a xenon ion extraction spectrum as measured with a Dresden EBIS-A for an ionization time of 5 s. In Fig. 17 a carbon ion extraction spectrum is shown as measured with a superconductiong Dresden EBIS-SC for an ionization time of 200 ms (for details see Ref. [31]).
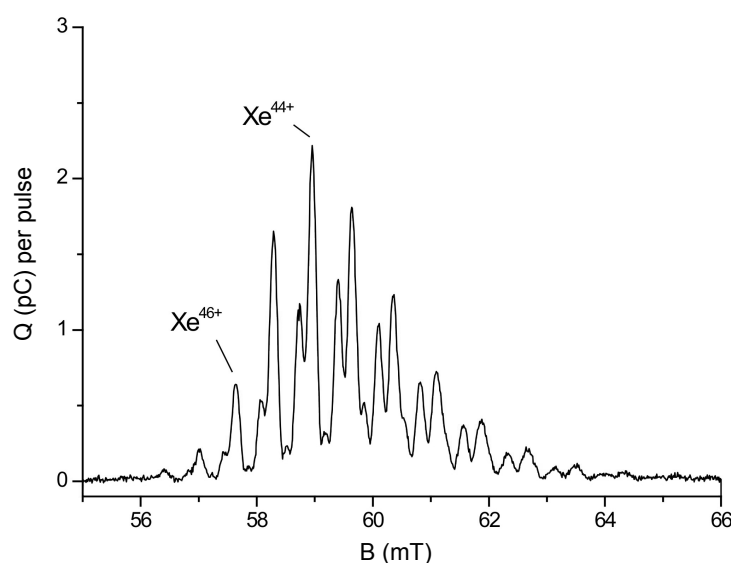

Fig. 16: A xenon ion extraction spectrum measured at a Dresden EBIS-A for a vacuum of 5×10^{-10} mbar, an electron beam energy of 12 keV and an electron beam current of 100 mA.

4.3 Ion beam separation using a Wien filter

A Wien filter is a particle separator with crossed magnetic and electric field configuration providing mass- and charge-state-separated beams of excellent quality and small spatial dimensions [32]. With the Wien filter as an ion source add-on, a very compact device is available substituting a complete standard beamline set-up with a space-consuming dipole magnet and other necessary equipment (see Fig. 18). The Wien filter can be used as a stand-alone solution for various beamline set-ups. Depending on the installed mass- and charge-state-separating aperture, a resolution of better than 80 is available. The geometrical dimensions of the Wien filter are small compared to a classical dipole magnet. The Wien filter fits easily on a beamline, making a change of the ion beam direction, as is necessary for a dipole magnet, obsolete.
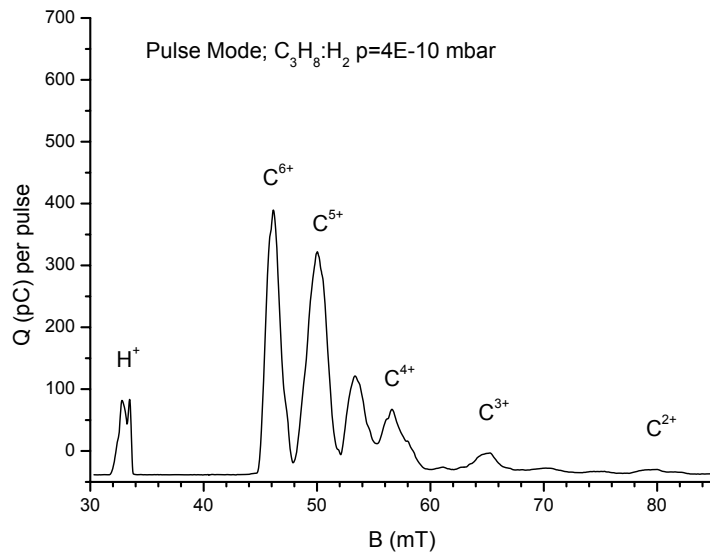
Fig. 17: A carbon ion extraction spectrum measured at a Dresden EBIS-SC for a vacuum of 4×10^{-10} mbar, an electron beam energy of 12 keV, an electron beam current of 400 mA and an ionization time of 200 ms.
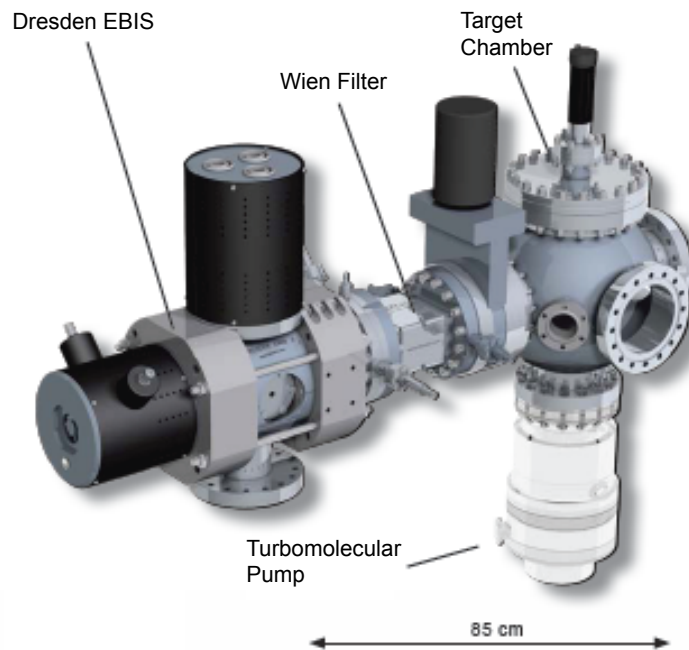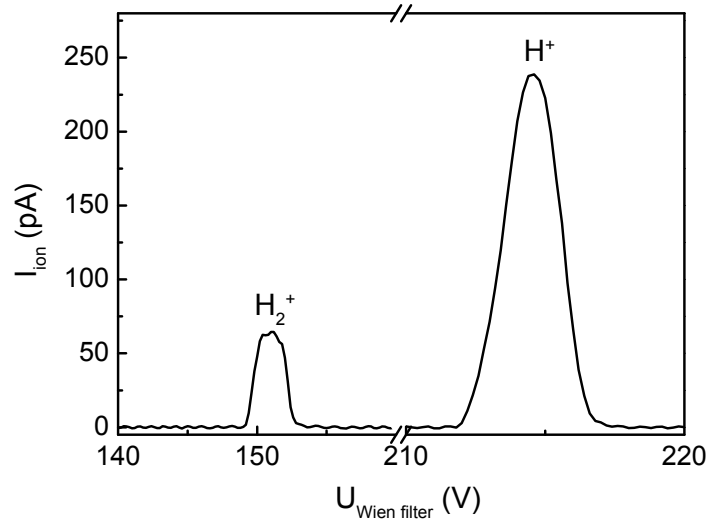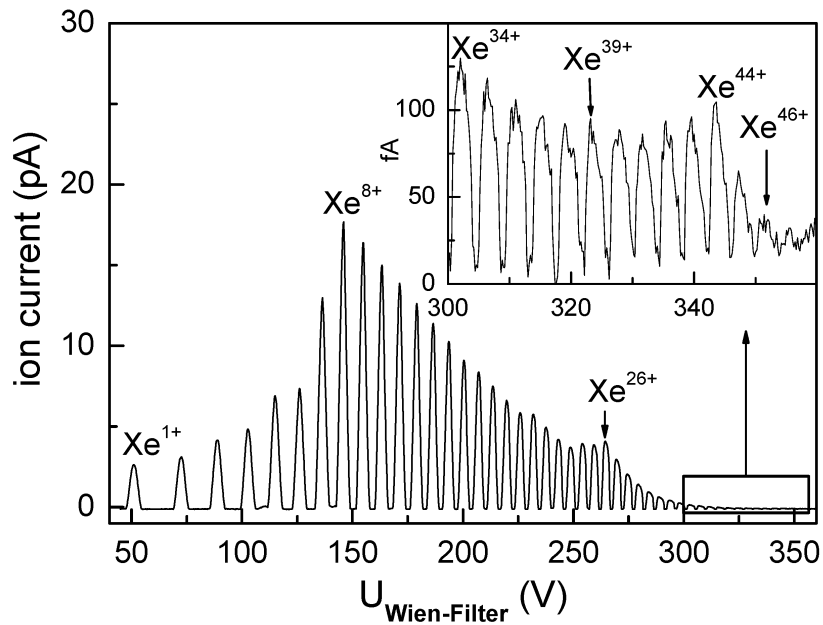

Fig. 18: A 3D presentation of a Wien filter-based beamline

The use of a Wien filter allows for separation of light and intermediate-Z ions of all ion charge states. For hydrogen and xenon, this is shown in Figs. 19 and 20. The most important difference to the use of analysing magnets is that a magnet has a gap of several centimetres, but for obtaining high resolution with a Wien filter we must work with aperture diameters in the millimetre or sub-millimetre region, i.e. beam losses through the Wien filter have to be taken into account.

Fig. 19: A leaky mode hydrogen ion extraction spectrum measured at a Dresden EBIS for a vacuum of 3×10^{-9} mbar, an electron beam energy of 13.6 keV and an electron beam current of 30 mA.

Fig. 20: A leaky mode xenon ion extraction spectrum measured at a Dresden EBIS for a vacuum of 3×10^{-9} mbar, an electron beam energy of 13.6 keV and an electron beam current of 30 mA.

4.4 Beams of singly charged molecular fragments and clusters

In leaky mode, EBISs can be used as sources for low charged ions from molecular fragments. The production of molecular fragments in an EBIS is of interest for various applications. This concerns issues such as studies on electronic transitions in molecules by spectroscopy of emitted electromagnetic radiation, protonation studies on complex molecules, as well as investigations on the interaction of molecular fragments with surfaces and on free molecules or gases in a corresponding gas jet. The use of a gas target may allow the production of neutral beams of different molecular fragments by charge exchange processes. Figure 21 shows an ion extraction from a Dresden EBIT after injection of propane. Thereby all possible stoichiometric ratios of propane fragments were detected. More details about molecule fragmentation in EBISs can be found in Ref. [33].
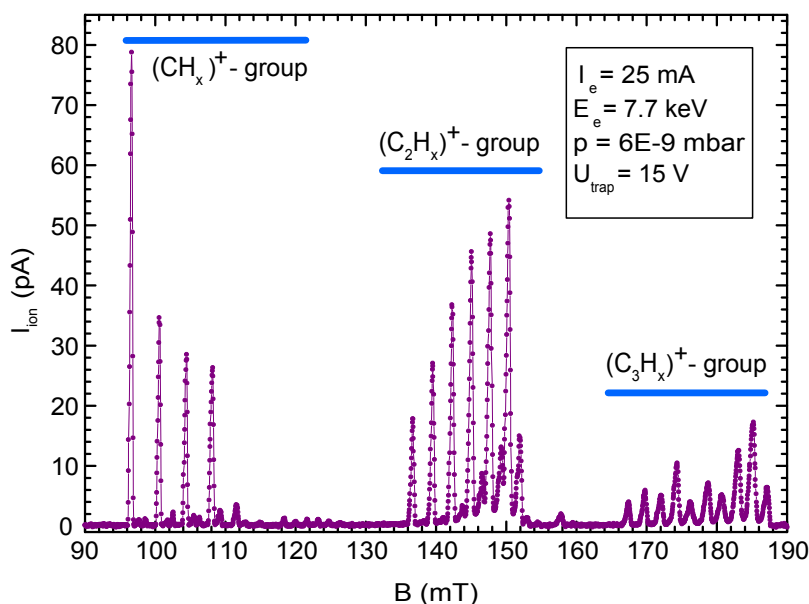

Fig. 21: Molecular fragment spectrum in leaky mode extracted from the Dresden EBIT after injection of propane

Additionally, one can also produce more complex structures such as metal clusters. In Fig. 22 this is shown for copper clusters as produced with a Dresden EBIT. The copper was introduced into the ion source by sputtering from a copper surface under gold ion irradiation. The capability of this technique is seen if we note that clusters with different isotope ratios can be clearly resolved, such as $[(^{63}Cu)_3]^{1+}$, $[(^{63}Cu)_2(^{65}Cu)_1]^{1+}$, $[(^{63}Cu)_1(^{65}Cu)_2]^{1+}$ and $[(^{65}Cu)_3]^{1+}$. Without a great deal of effort, cluster beam currents of up to 10^5 clusters per second were measured.

4.5 Absolute numbers of extracted ions

To characterize the potential of different EBIS types, we give some absolute ion numbers for pulsed ion extraction of ion sources of the Dresden EBIS type in Table 3. The summarized numbers characterize the expected order of magnitude for ion extraction but can deviate in their dependence on the individual ion source and the selected operation regime.
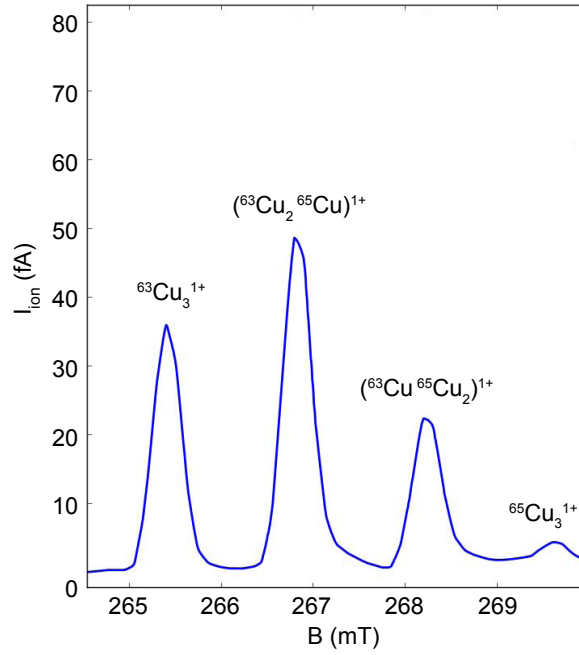
Fig. 22: Measured copper clusters from a Dresden EBIT at an electron beam energy of 6 keV and an electron beam current of 23 mA.

Table 3: Ions per pulse for pulsed ion extraction of ion sources of the Dresden EBIS type.

Ion	Dresden EBIT	Dresden EBIS	Dresden EBIS-A	EBIT : EBIS : EBIS-A
C^{6+}	10 000 000	30 000 000	400 000 000	1 : 3 : 40
Ar^{16+}	900 000	8 000 000	250 000 000	1 : 9 : 280
Ar^{18+}	6000	90 000	1 500 000	1 : 15 : 250
Xe^{44+}	10 000	700 000	10 000 000	1 : 70 : 1000

4.6 Pulse shape for typical ion extraction

Typical pulse widths at pulsed ion extraction from an EBIS are of the order of a few microseconds. Thereby the pulses are not completely symmetric but have a tail on the side of higher flight times. The reason is that, at the moment of trap opening, only those ions are extracted that have a flight direction towards the extraction side. All other ions will be reflected at the potential wall at the gun side and extracted after that. This situation is shown in Fig. 23. The absolute pulse width is determined by the speed of switching the trap potential at the extraction side ('slew rate'). We see that we can influence the pulse width from some microseconds up to about 100 μs, i.e. we come near to 'flat-top' pulses. As an example this is shown in Fig. 24 for ion pulses from a Dresden EBIS-A with a trap length L of 6 cm and different slew rates.

4.7 Short-time ion pulse extraction

For some applications the time structure of the extracted beams of HCIs is of fundamental interest. For example, for applications in time-of-flight secondary ion mass spectroscopy (TOF-SIMS) and in some solid-state physics experiments, the formation of short pulses up to the nanosecond range is of interest. Present studies prove that a short pulsed ion extraction from the Dresden EBIT is possible. The extracted
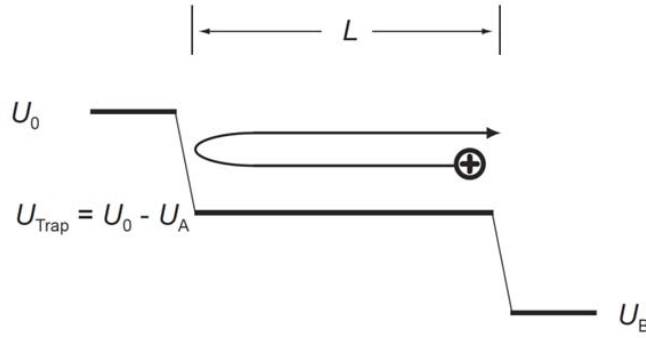
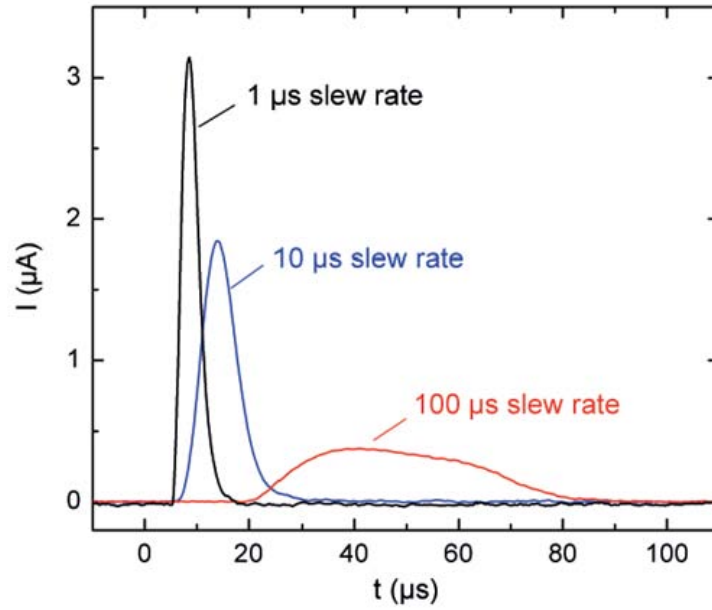**Fig. 23:** Ion paths at the moment of ion extraction

Fig. 24: Carbon ion pulses from a Dresden EBIS-A for different slew rates

ion charges per pulse are in the range of some femtocoulombs and it is possible to extract several pulses until the trap has to be reloaded. The maximum extracted ion charge depends significantly on the chosen extraction time. As an example we show in Fig. 25 a plot of extracted ion charges for an Ar^{16+} pulse as a function of the extraction time t_{extr}. From Fig. 25 it is seen that, after some hundreds of nanoseconds, the extracted ionic charge increases no further.

4.8   Ion beam emittance

For applications of ion beams, a quantitative measure of the quality of the beam is given by the root-mean-square (r.m.s.) emittance

$$\varepsilon_{x,\text{rms}} = \sqrt{\overline{x^2}\,\overline{x'^2} - \overline{x'^2}} \tag{34}$$

in x–x' trace space and equivalently in the case of y–y'.

A common method to determine these ion beam parameters is the pepperpot technique, which can be traced back to works of the 1960s [35]. A scheme of a pepperpot emittance meter is shown in Fig. 26. The incoming ion beam passes the pepperpot mask and is separated into several beam spots. The particles hitting the microchannel plate (MCP) create an electron current, which is amplified passing
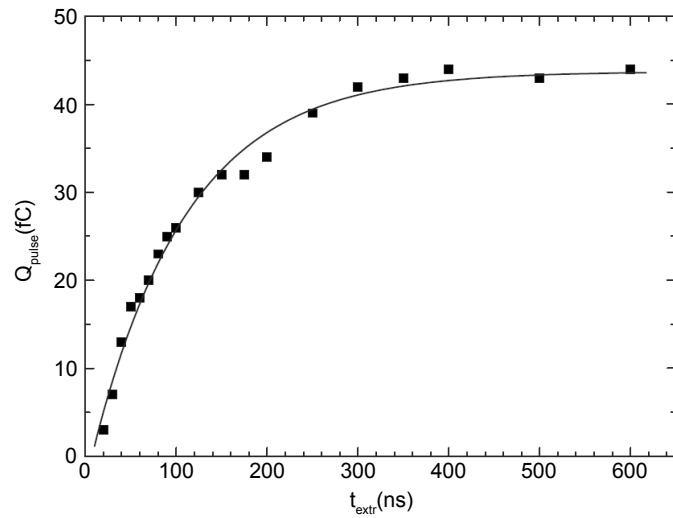
Fig. 25: Extracted ion charges of Ar^{16+} pulses from a Dresden EBIT as a function of the extraction time t_{extr} (after Ref. [34]).

the two MCPs. The electrons are then accelerated towards the phosphor screen. The visible light spots created at the phosphor screen are detected after $90°$ deflection by a CCD camera. The emittance of the ion beam can be determined from the positions, sizes and shapes of the light spots.
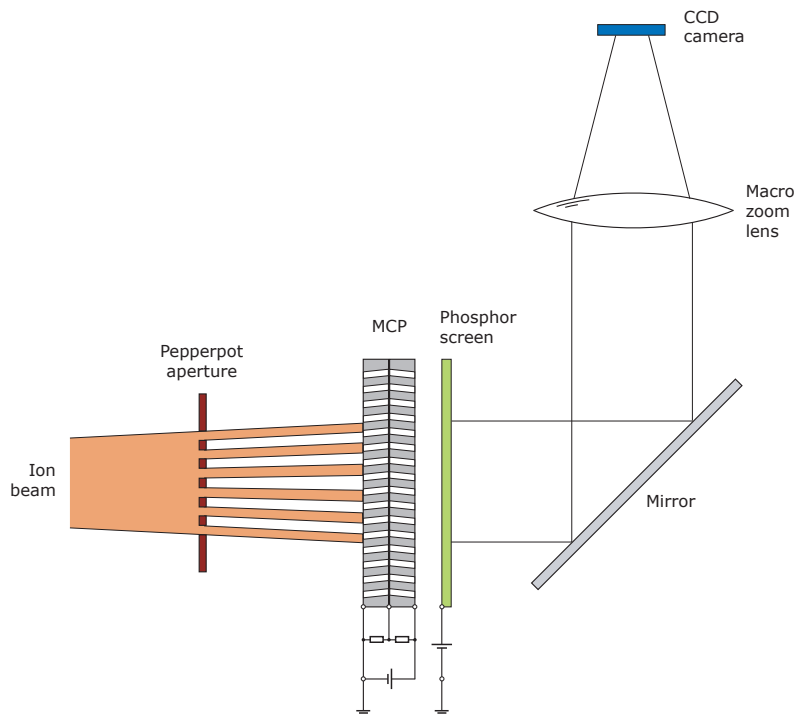

Fig. 26: Scheme of a pepperpot emittance meter

Because of the small ionization volume and the small electron beam diameter, EBISs produce ion beams with very low emittances. As an example in Fig. 27 the x and y r.m.s. emittance for C^{6+} ions

extracted from a Dresden EBIS-A is shown as a function of the electron beam current. Typical emittances are of the order of some mm mrad.
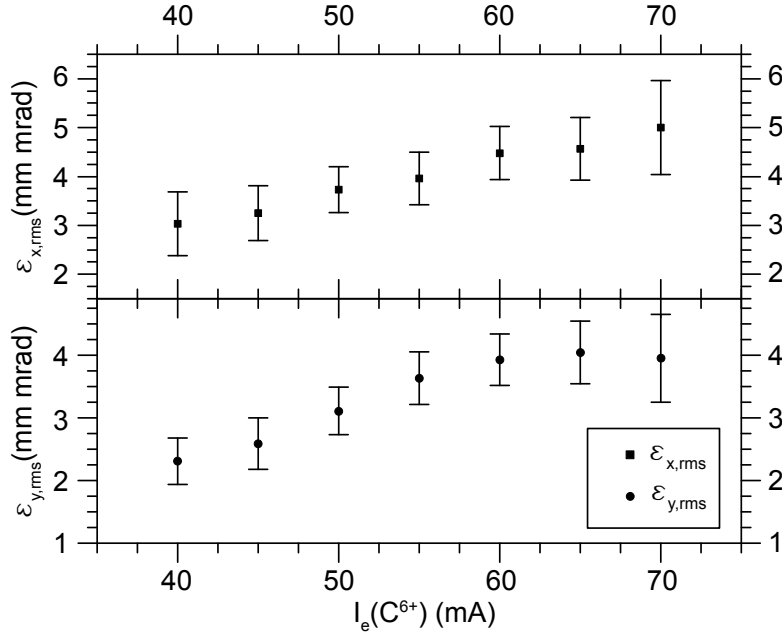

Fig. 27: R.m.s. emittance of C^{6+} ions extracted from a Dresden EBIS-A

For higher beam energies, the pulse components perpendicular to the beam direction are small compared with the pulse components in the beam direction, i.e. higher beam energies lead to lower emittances. This can be described by the normalized emittance and it yields

$$\varepsilon_{\mathrm{norm}} = \beta'\gamma'\varepsilon \qquad \text{with} \quad \beta' = \frac{v}{c} \quad \text{and} \quad \gamma' = \frac{1}{\sqrt{1-\beta^2}}, \tag{35}$$

where v is the ion velocity and c is the speed of light. For typical operation regimes of EBISs, the normalized emittance is of the order of 10^{-3} mm mrad.

4.9   Energy spread and absolute energy of extracted ions

In order to measure the absolute energy and the energy spread of extracted ions, a retarding field analyser (RFA) can be applied. An RFA is an electrostatic energy analyser that allows the kinetic energy distribution of an ion beam to be measured. The analyser consists of a collimator with exchangeable apertures, three meshes, with the central mesh set on high potential, and a Faraday cup for current measurement.

The ion or electron current is measured in the Faraday cup of the RFA. In order to analyse the energy distribution of the incoming ion beam, the potential of the retarding mesh is increased stepwise while measuring the current in the cup. The measured dependence $I_{\mathrm{ion}}(U_{\mathrm{RFA}})$ is differentiated and fitted with a Gaussian to obtain the energy distribution. The mean energy of the charged particles E_{m} is defined as the centre position of the Gaussian. The energy spread of the charged particle beam ΔE is defined as the full width half-maximum (FWHM) of the Gaussian.

Figures 28 and 29 show examples of measured absolute energies and energy spread of ions extracted from a Dresden EBIS-A. The energy spread of the ion beam, which depends on the electron beam current, is generally quite small for Dresden EBIS/T systems. For the Dresden EBIS-A, it is of the order of several electronvolts. More details about the RFA technique can be found in Ref. [36].
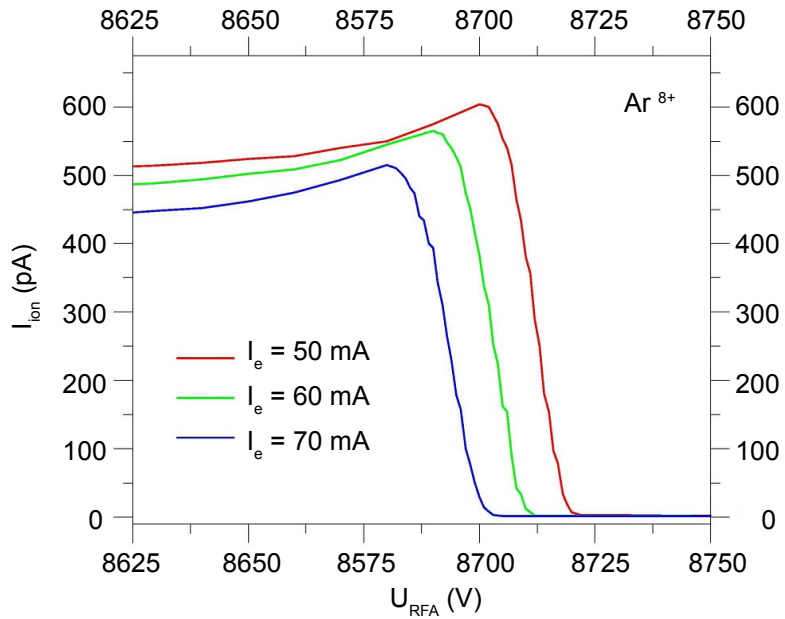
Fig. 28: Plot showing $I_{\mathrm{ion}}(U_{\mathrm{RFA}})$ curves for electron currents of 50, 60 and 70 mA measured with Ar^{8+} at a drift tube potential of 8.7 keV at a Dresden EBIS-A.
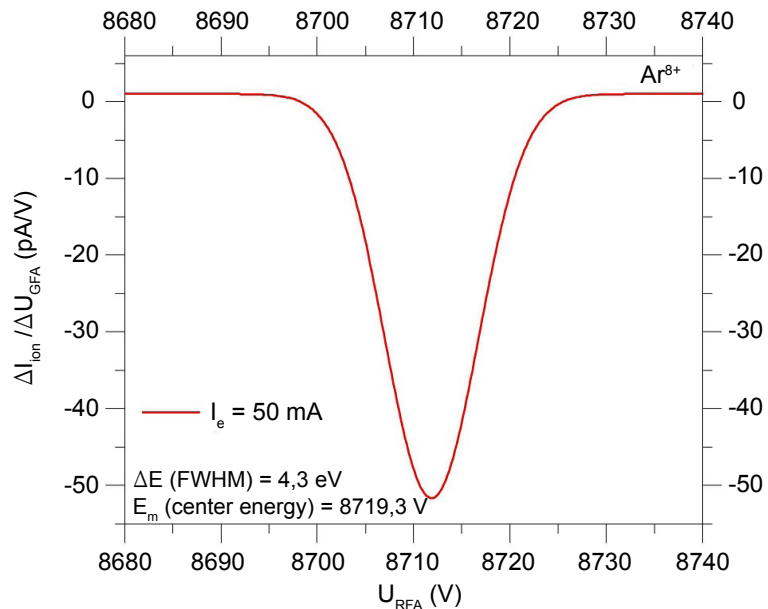

Fig. 29: The energy distribution of the extracted ion beam is $E = 4.3\,\mathrm{eV}$ at an electron beam of $I_{\mathrm{e}} = 50\,\mathrm{mA}$ measured at a Dresden EBIS-A.

5   EBISs as sources of X-rays from HCIs

5.1   X-ray emission from HCIs

EBISs are excellent tools for X-ray spectroscopy of highly charged ions. X-rays from HCIs are of fundamental interest for atomic physics, plasma diagnostics, astrophysics and other applications. In contrast to other sources of X-rays from HCIs such as hot plasmas or accelerator facilities, EBISs are comparatively small and low-cost devices. Additionally, they offer the possibility to control the electron beam energy very precisely, which creates superior conditions for advanced experiments studying X-rays from HCIs.

It is well known that vacancies in the atomic shell influence X-ray lines in terms of their transition energies, transition probabilities and the structure of the measured spectrum. Classical X-ray spectra have been known for more than 100 years. As long ago as 1917 Barkla received a Nobel Prize for the discovery of characteristic X-rays. Less than 50 years later, in 1962, the first X-ray source outside our Solar System was observed and from that date interest in X-rays from HCIs has grown more and more.

Compared to classical X-rays as parent diagram lines appearing after the production of an inner-shell vacancy and subsequent filling of this vacancy with an outer electron, X-rays from HCIs can be different from these classical transitions. Mainly, we can observe X-ray transitions from

- direct excitation (DE),
- radiative recombination (RR) and
- dielectronic recombination (DE).

Detailed information on the basic physics of X-rays from HCIs can be found, for example, in Refs. [37] and [38]. Measurements were performed by different groups working with EBISs – the pioneering work of the Livermore group of Dr. Beiersdorfer *et al.* should be pointed out especially (see e.g. Ref. [39]).

5.2   X-ray measurements

Measurements show that in the case of the Dresden EBIT individual dipole lines have a radiation power of the order of some nanowatts. For the Dresden EBIS-A this power increases by about one order of magnitude and for the superconducting Dresden EBIS-SC by a factor of about 200. As a rule, the number of X-rays emitted is high enough to perform energy-dispersive as well as wavelength-dispersive X-ray spectrometry in acceptable time frames of minutes up to some hours.

In Fig. 30 a measured wavelength-dispersive DE spectrum from carbon- to helium-like iron ions is shown. The measurement was realized with a flat crystal and for an electron beam current of 40 mA. Figure 31 shows an argon RR spectrum as measured with a Dresden EBIT. Here the electron capture into the highest possible argon charge state is shown with a clear signature.

DE as well as RR measurements can be realized with comparatively simple detection techniques. In both cases, without any synchronization with the EBIS, a detector can measure the emitted X-rays passing through a spectroscopic window. More sophisticated are measurements of DE processes where the measurement process must be synchronized with the electron beam energy because DE processes are sharp resonance processes. For example, in Fig. 32 a krypton DE KLL spectrum for Kr^{28+} up to Kr^{32+} ions is shown.

In addition to the classical energy- or wavelength-dispersive X-ray spectroscopy, time-resolved X-ray spectrometry is possible if we add to each measured count time information about the ionization time in the ion trap (time between closing the ion trap and registration of the X-ray quanta). Such a spectrum is shown in Fig. 33 for a Kr^{28+} DE KLL X-ray transition. The figure shows the evolution of the Kr^{28+} ionization charge state in the ion trap of a Dresden EBIT and demonstrates that such ions can be stored for 10 s or longer.
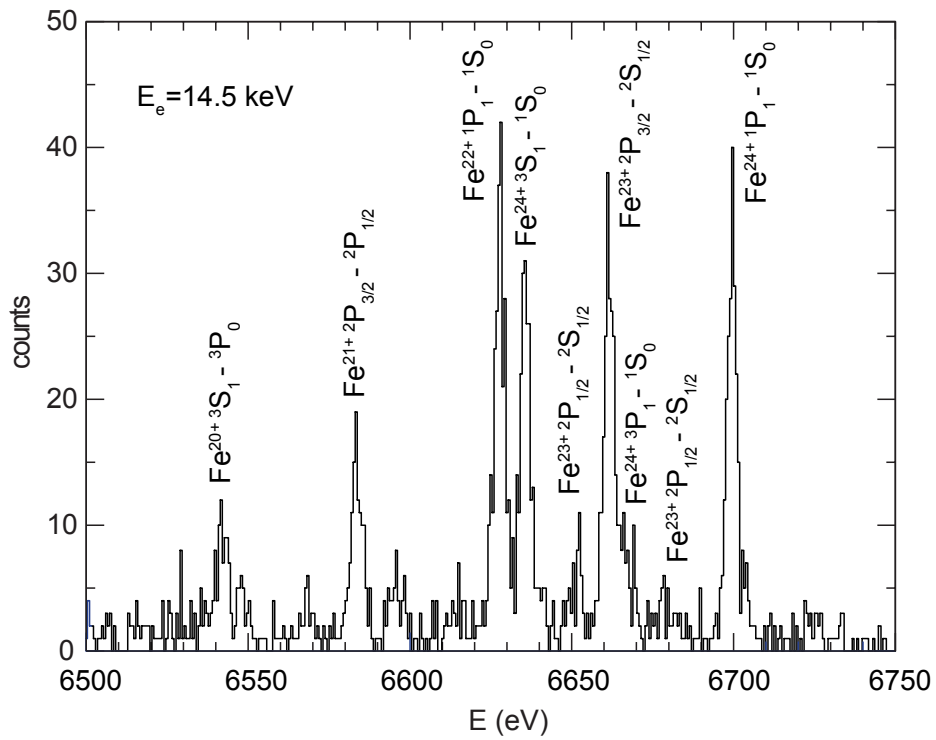
Fig. 30: Wavelength-dispersive iron X-ray spectrum from DE processes in a Dresden EBIT at 14.5 keV electron beam energy.
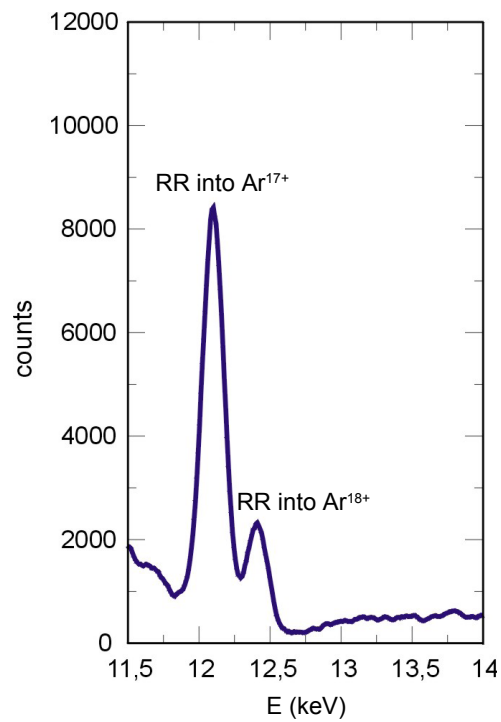

Fig. 31: Energy-dispersive measured argon RR spectrum from a Dresden EBIT for the electron capture into hydrogen-like and bare argon at an electron beam energy of 8 keV and an electron beam current of 15 mA.
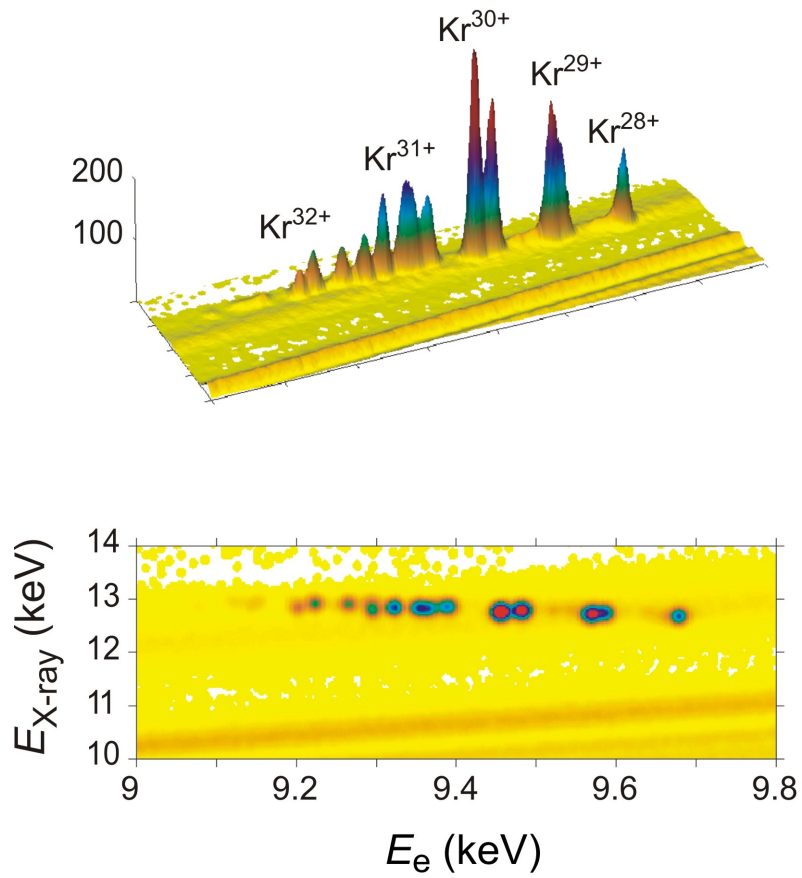
Fig. 32: Krypton KLL spectrum from DE processes for Kr^{28+} up to Kr^{32+} ions in a Dresden EBIT
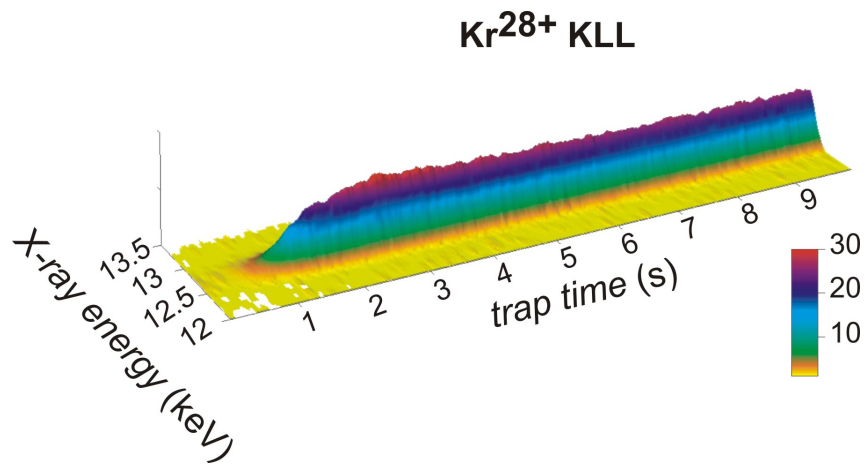

Fig. 33: Time-resolved krypton DE KLL spectrum for Kr^{28+} measured at a Dresden EBIT

6 Applications of EBISs (selected topics)

As mentioned at the beginning, EBISs are versatile tools for investigations on HCIs in basic and applied research as well as for applications with strong practical relevance. It is not the aim of the present chapter to discuss all these topics in detail, but in the following subsections we will give some examples of the versatile application potential of HCIs.

6.1 HCI-FIB for structuring and surface analysis

Standard focused ion beam (FIB) systems use liquid metal ion sources (LMISs) with their rather small standard spectrum of projectiles. Combining an EBIS, which provides a broader palette of ion species from different elements (from noble gases up to metals) ranging from high to low charge states, with an FIB column leads to new useable physical properties and new applications.

As already mentioned, the potential energy stored in the highly charged ions due to the ionization process leads to power densities of order 10^{12} up to 10^{14} W cm^{-2} in single ion–surface interactions and therefore to higher yields of secondary ions and secondary electrons per incident ion compared to conventional ions. Preliminary experiments have been done at the CNRS in Marcoussis [40].

Furthermore, the ion implantation range can be varied by selecting a certain charge state, which is due to the final kinetic energy at a constant acceleration potential (see Fig. 34). This can be realized via the integration of a crossed-field ion beam separator, the already introduced Wien filter [32], which enables the user to separate ions according to their mass-to-charge ratio. Since the ion energy depends on the charge state as well as on the mass, a broad range of projectile energies is available. Also, the intrinsic potential energy of the projectile can be adjusted by the user by selecting the charge state of the ions.
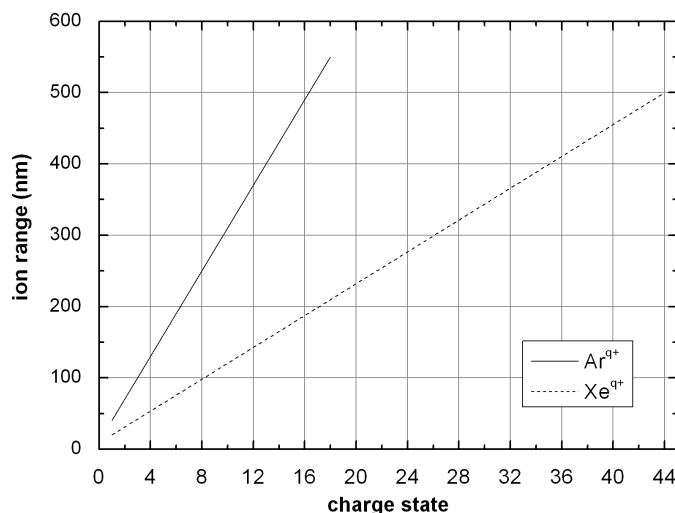

Fig. 34: Ion range of argon and xenon ions in silicon at different kinetic energies

The technology as described above complements the classical spectrum of projectiles for various applications beyond the latest developments using noble gas ions in FIB systems. Considering the ion charge state as a new physical parameter that can be varied offers suitable preconditions in sputtering processes with regard to the produced secondary particles being used for surface analysis (TOF-SIMS). This also takes into account the ability to vary the kinetic energy at a fixed acceleration potential of the ion source and FIB column assembly.

6.2 Particle therapy

Cancer is the second most common cause of death worldwide and, statistically, about 33% of all inhabitants of the European Union will be confronted with some kind of cancer in their lives. Currently about 45% of all cancer cases can be treated, mainly by surgery and/or by radiation therapy [41].

Within radiotherapy, radiation with hadrons (mainly protons and carbon ions) is the most promising treatment technique. In contrast to the classical irradiation with X-rays, treatment with ions has significant advantages. Energy deposition within the tissues obeys the Bragg interaction law, i.e. the maximum of the energy is deposited at the end of the particle trajectories, hence in the tumour cells. The ion range can be adjusted precisely by varying the kinetic energy of the particles. The intruding ions lose energy inside a dense medium according to the Bragg curve. Most of the kinetic energy is deposited at a certain depth along the ion path. This effect can be used to destroy a tumour while the healthy tissue around is spared (this is important for tumours in the vicinity of risky organs like the medulla).

Another important property of ions as opposed to photons is their electrical charge. Charged particles can be focused and deflected by electrical and magnetic fields, providing the ability to scan with the ion beam over the tumour very precisely. Owing to the variation of the kinetic energy of the ions, it is possible to vary the penetration depth. Hence the tumour can be scanned voxel by voxel (a voxel is a three-dimensional volume element). Besides the electrical properties, the relative biological efficiency (RBE) of the ions is higher by a factor of about 3. This means that the same dose of carbon ions affects the tumour tissue by a factor of 3 more compared to classical X-rays. A higher RBE allows a lower dose to produce the same effect on the tumour with less damage to the healthy tissue.

Nowadays, a substantial number of medical particle therapy facilities are based on synchrotron accelerators combined with ECR ion sources. Owing to the low purity of the ion beam, electron strippers are required. If using an EBIS ion source and its excellent beam purity, a subsequent electron stripper is no longer necessary. Also, the lower emittance of EBIS sources will lead to a higher transparency of the accelerator structure. For other accelerator strategies, like direct wall accelerators or direct driven accelerators, even the application of room-temperature EBIS ion sources might be possible.

6.3 Charge breeding

In nuclear mass measurements involving ions stored in Penning traps, the precision of the experimental method increases proportionally with the charge state of the investigated ions. Furthermore, for proposed nuclear fusion reaction studies, neutron-rich, relatively short-lived radioactive isotopes have to be accelerated to energies above the Coulomb barrier, which requires a small mass-to-charge ratio (A/q) to reduce the scale and cost of the accelerator. These and other endeavours rely on the availability of HCI from a broad spectrum of elements or even exotic radioactive species, respectively.

As described above, EBISs or EBITs are HCI sources which have many advantages. However, they are typically loaded via gas injection, which limits the range of available ion species from these machines. The injection of externally produced low charged ions into an EBIS or EBIT and re-extraction as HCIs, known as charge breeding, offers a way to increase the range of available HCI species. Various ion injection techniques have been used for charge breeding. Among these are experimental set-ups including metal vapour vacuum arc and liquid metal or liquid metal ion sources [42, 43] but also beams of short-lived radioactive isotopes produced using the isotope separation on-line (ISOL) technique [44].

Recently, a Dresden EBIS-A was fed by a liquid metal alloy ion source to produce HCI from low charged gold ions. For the charge-bred Au^{q+} ions, charge states up to $q = 60$ were achieved (see Fig. 35). This experimental technique represents a clean and elegant way of introducing metals or other elements into the Dresden EBIS-A that cannot be injected directly through a gas valve. Therefore, the range of applications for this type of ion source is extended.
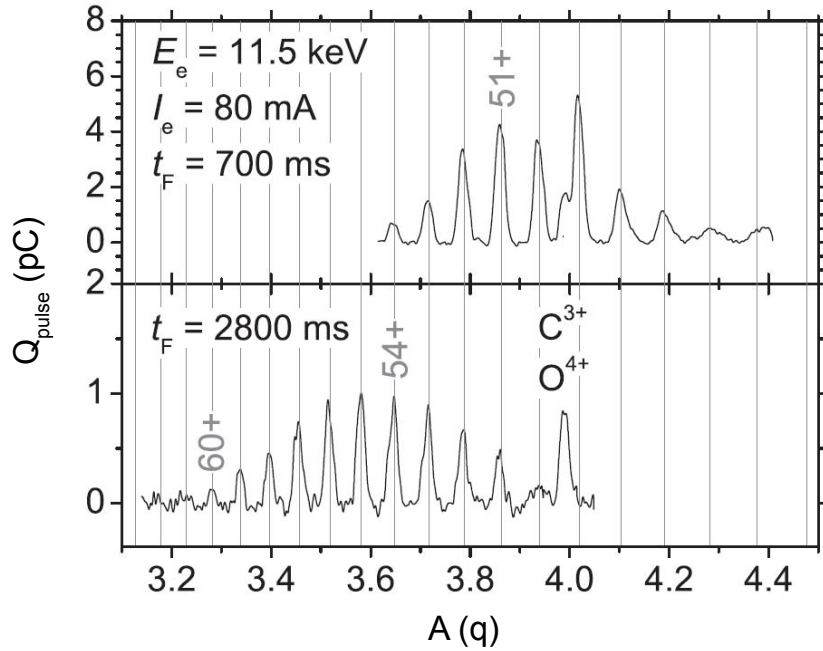
Fig. 35: Charge breeding spectra with gold ions injected into the trap of an EBIS-A with an external LMIS (from Ref. [45]).

7 Conclusion

Highly charged ions (HCIs) are becoming more and more important in basic research as well as technological applications (for example see Refs. [46] – [48]). This is because of their unique properties, which are listed briefly at the beginning of this chapter. In the past, large accelerator devices had to be used for the production of HCIs, while today's sources of HCIs will fit on a table top. This increases the availability of HCIs and opens up new possibilities for a larger community to realize experiments with HCIs.

This chapter has highlighted the electron beam ion source (EBIS) technology as an efficient and elegant way to produce HCIs. The basic physics and working principle of EBISs are explained in detail and compared to other existing HCI sources. Especially, aspects of HCI extraction but also the use of EBISs as sources of X-rays from HCIs trapped inside the machines are discussed.

We hope this work inspires researchers to continue the advancement of this extraordinary ion source technology and creates ideas for new fields of applications of HCIs produced by EBISs in the future.

References

[1] I. S. Bowen and R. A. Millikan, *Phys. Rev.* **25** (1925) 591.

[2] B. Edlen, *Z. Astrophys.* **22** (1942) 30.

[3] R. Geller, *Electron Cyclotron Resonance Ion Sources and ECR Plasmas* (IOP Publishing, Bristol 1996).

[4] B. Sharkov, Laser ion sources, in *The Physics and Technology of Ion Sources*, 2nd edn. (Wiley-VCH, Weinheim, 2004).

[5] J. Gillaspy, *Trapping Highly Charged Ions: Fundamentals and Applications* (Nova Science, Huntington, NY, 2001).

[6] F. Currell, Electron beam ion traps and their use in the study of highly charged ions, in *The Physics of Multiply and Highly Charged Ions*, Ed. F. Currell (Kluwer Academic, Dordrecht, 2003), Vol. I.

[7] J. Gillaspy, *J. Phys. B: At. Mol. Opt. Phys.* **34** (2001) R93.

[8] H. F. Beyer and V. P. Shevelko, *Introduction to the Physics of Highly Charged Ions* (IOP Publishing, Bristol, 2003).

[9] E. D. Donets, USSR Inventor's Certificate No. 248860, 16.03.1967; *Bull. OIPOTZ* **24** (1969) 65.

[10] E. D. Donets, V. I. Ilushenko and V. A. Alpert, Ultrahigh vacuum electron beam ion source of highly stripped ions, Proc. First Int. Conf. on Ion Sources, Saclay, France, 1969, p. 635.

[11] E. D. Donets and V. P. Ovsyannikov, *Sov. Phys. JETP* **53** (1981) 466.

[12] M. A. Levine, R. E. Marrs, J. R. Henderson, D. A. Knapp and M. B. Schneider, *Phys. Scr.* **T22** (1981) 157.

[13] J. W. McDonald and D. H. G. Schneider, *Nucl. Instrum. Methods Phys. Res.* **B241** (2005) 870.

[14] V. P. Ovsyannikov and G. Zschornack, *Rev. Sci. Instrum.* **70** (1999) 2646.

[15] For EBIT/EBIS ion sources of the Dresden EBIT/EBIS family see: `http://www.dreebit.com`.

[16] G. Zschornack, V. P. Ovsyannikov, F. Grossmann, A. Schwan and F. Ullmann, Proc. Int. Symp. on Electron Beam Ion Sources and Traps, Stockholm, Sweden, 7–10 April 2010; JINST 5 C08012.

[17] R. Becker and O. Kester, *Rev. Sci. Instrum.* **81** (2010) 02A513.

[18] V. P. Ovsyannikov, Technique and application of electron beam ion sources, Doctoral thesis, Joint Institute of Nuclear Research, Dubna, Russia, 1996.

[19] W. Lotz *et al.*, *Z. Phys.* **206** (1967) 205.

[20] T. Werner, Diploma thesis, Institut fuer Kern- und Teilchenphyik, TU Dresden, Dresden, Germany, 1997.

[21] A. Mueller and R. Frodel, *Phys. Rev.* **44** (1980) 29.

[22] A. Mueller and E. Salzborn, *Phys. Lett.* **A59** (1976) 19.

[23] F. Ullmann, Ph.D. thesis, Technische Universitaet Dresden, Fakultaet Mathematik und Naturwissenschaften, Dresden, Germany, 2005.

[24] Y. S. Kim and R. H. Pratt, *Phys. Rev.* **A27** (1983) 2913.

[25] R. Becker, Talk Int. Conf. on Ion Sources (ICIS 2009), Gatlinburg, TN, USA, September 2009.

[26] B. M. Penetrante, J. N. Bardsley, D. DeWitt, M. Clark and D. Schneider, *Phys. Rev.* **A43** (1991) 4861.

[27] I. V. Kalagin, D. Kuechler, V. P. Ovsyannikov and G. Zschornack, *Plasma Sources Sci. Technol.* **7** (1998) 441.

[28] G. Herrmann, *J. Appl. Phys.* **29** (1958) 127.

[29] H. Kuramoto, T. Kinnugawa, H. Watanabe, C. Yamada, S. Ohtani, I. Yamada and F. J. Curell, *Rev. Sci. Instrum.* **73** (2002) 42.

[30] A. Thorn, Ph.D. thesis, Technische Universitaet Dresden, Fakultaet fuer Mathematik und Naturwissenschaften, Dresden, Germany, 2012.

[31] G. Zschornack, A. Schwan, F. Ullmann, F. Grossmann, V. P. Ovsyannikov and E. Ritter, *Rev. Sci. Instrum.* **83** (2012) 02A507.

[32] M. Schmidt, H. Peng, G. Zschornack and S. Sykora, *Rev. Sci. Instrum.* **80** (2009) 063301.

[33] M. Kreller, G. Zschornack, U. Kentsch and R. Heller, *Rev. Sci. Instrum.* **79** (2008) 02A702.

[34] U. Kentsch, G. Zschornack, A. Schwan and F. Ullmann, *Rev. Sci. Instrum.* **81** (2010) 02A507.

[35] L. E. Collins and P. T. Stroud, *Nucl. Instrum. Methods* **26** (1964) 157.

[36] E. Ritter, Diploma thesis, Technische Universitaet Dresden, Department of Physics, Dresden, Germany, 2010.

[37] H. F. Beyer, H.-J. Kluge and V. P. Shevelko, *X-Ray Radiation of Highly Charged Ions* (Springer, Berlin, 1997).

[38] F. J. Currell (Ed.), *The Physics of Multiply and Highly Charged Ions* (Kluwer Academic, Dordrecht, 2003), Vol. I.

[39] P. Beiersdorfer, *AIP Conf. Proc.* **389** (1997) 121.

[40] F. Ullmann, F. Grossmann, V. P. Ovsyannikov, J. Gierak and G. Zschornack, *Appl. Phys. Lett.* **90** (2007) 083112.

[41] T. Auberger, E. Griesmayer, Das Projekt MedAustron - Designstudie, Fotec - Forschungs- und Technologietransfer GmbH, Wiener Neustadt, 2004 (chapter 1).

[42] N. Nakamura, T. Kinugawa, H. Shimizu, H. Watanabe, S. Ito, S. Ohtani, C. Yamada, K. Okazaki, M. Sakurai, M. R. Tarbutt and J. D. Silver, *Rev. Sci. Instrum.* **71** (2000) 684.

[43] A. Pikin, J. G. Alessi, E. N. Beebe, A. Kponou and K. Prelec, *Rev. Sci. Instrum.* **77** (2006) 03A909.

[44] F. Wenander, *J. Instrum.* **5** (2010) C10004.

[45] A. Thorn, E. Ritter, F. Ullmann, W. Pilz, L. Bischoff and G. Zschornack, *Rev. Sci. Instrum.* **83** (2012) 02A511.

[46] R. W. Schmieder and R. J. Bastasz, Proc. 6th Int. Conf. on the Physics of Highly Charged Ions, *AIP Conf. Proc.* **274**, Manhattan, KS, 1992.

[47] G. Zschornack, F. Grossmann, V. P. Ovsyannikov, R. Heller, U. Kentsch, M. Kreller, M. Schmidt, A. Schwan, A. Silze and F. Ullmann, *Materialwissenschaften und Werkstofftechnik* **40**(4) (2009) 1.

[48] V. Shevelko and H. Tawara (Eds.), *Atomic Processes in Basic and Applied Physics* (Springer, Heidelberg, 2012).